CHALMERS
UNIVERSITY OF TECHNOLOGY

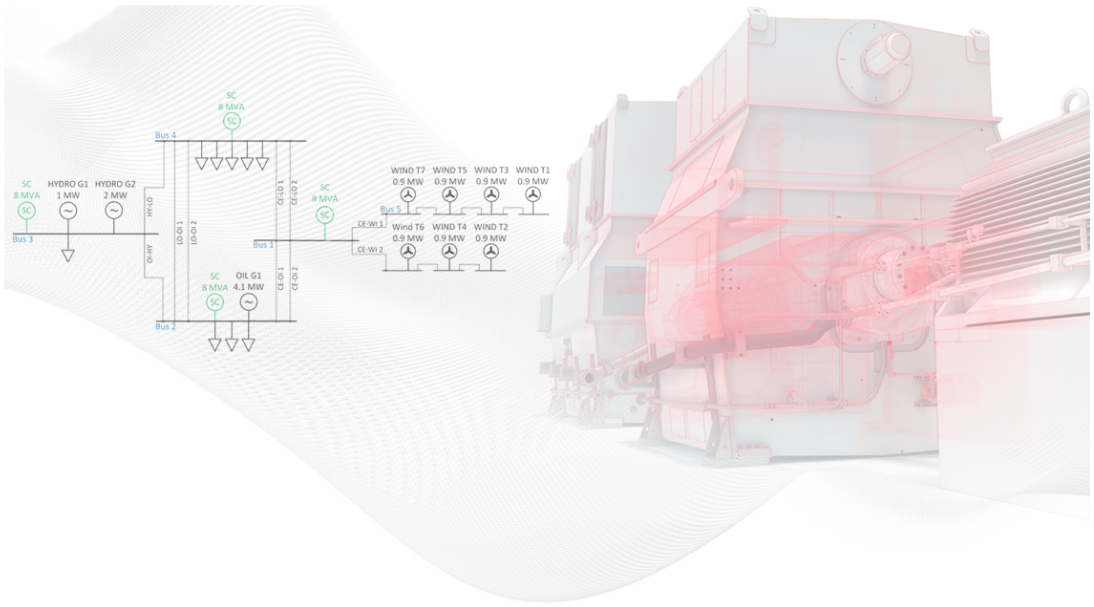

Evaluation of Synchronous Condensers in Modern Power Grids for Enhancing Grid Stability

A Comparative Study of the Performance in Different Grid Topologies

Master's thesis in Sustainable Electric Power Engineering and Electromobility

ANNA JOHANSSON
AMANDA SCHOBERG

DEPARTMENT OF ELECTRICAL ENGINEERING
CHALMERS UNIVERSITY OF TECHNOLOGY
Gothenburg, Sweden 2025
www.chalmers.se

Master's thesis 2025

Evaluation of Synchronous Condensers in Modern Power Grids for Enhancing Grid Stability

A Comparative Study of the Performance in Different Grid Topologies

ANNA JOHANSSON
AMANDA SCHOBERG

CHALMERS
UNIVERSITY OF TECHNOLOGY

Department of Electrical Engineering
Division of Electric Power Engineering
Chalmers University of Technology
Gothenburg, Sweden 2025

Evaluation of Synchronous Condensers in Modern Power Grids for Enhancing Grid Stability
A Comparative Study of the Performance in Different Grid Topologies
ANNA JOHANSSON
AMANDA SCHOBERG

© ANNA JOHANSSON, AMANDA SCHOBERG 2025.

Supervisors: Gunnar Porsby & Carl Nilsson, ABB
Examiner: Massimo Bongiorno, Department of Electric Power Engineering

Master's Thesis 2025
Department of Electrical Engineering
Division of Electric Power Engineering
Chalmers University of Technology
SE-412 96 Gothenburg
Telephone +46 31 772 1000

Cover: A diagram of a power grid (left) and a synchronous condenser (right).

Typeset in LaTeX
Printed by Chalmers Reproservice
Gothenburg, Sweden 2025

Evaluation of Synchronous Condensers in Modern Power Grids for Enhancing Grid Stability
A Comparative Study of the Performance in Different Grid Topologies
ANNA JOHANSSON
AMANDA SCHOBERG
Department of Electrical Engineering
Chalmers University of Technology

Abstract

As renewable energy sources increasingly replace conventional synchronous generation, the resulting decline in system inertia and reactive power capability presents growing challenges for maintaining power system stability. Synchronous condensers (SCs) offer a potential solution by enhancing voltage stability through high fault current injection, providing dynamic reactive power support, and contributing to frequency stability via rotational inertia. This thesis investigates the ability of SCs to improve power system stability, with a focus on voltage regulation and frequency support. Simulations were conducted in DIgSILENT PowerFactory on two grid models of varying strength and complexity, referred to as the robust grid and the islanded grid. Three SC ratings, 8 MVA, 67 MVA, and 200 MVA, were evaluated to determine their effectiveness under different fault scenarios and deployment strategies.

In the robust grid model, SCs had a limited impact on mitigating voltage dips due to the high short-circuit capacity (SCC) of the system and in the case of a short distance between the SC and the fault. However, notable voltage recovery improvements were observed under weakened grid conditions and at more vulnerable locations. Performance between the 67 MVA and 200 MVA units was similar, though deploying multiple smaller SCs may provide redundancy benefits. Regarding frequency support, the high system inertia in the robust grid limited improvements in the rate of change of frequency (RoCoF) and frequency nadir, which were more evident in the islanded model. In the weaker islanded system, the deployment of an 8 MVA SC significantly improved both voltage and frequency stability. The SC effectively mitigated voltage dips, enhanced voltage recovery, and improved the RoCoF and frequency nadir during disturbances. Its positive impact was consistent across all placement locations, making the deployment strategy less critical. These results highlight the value of SCs in supporting voltage and frequency stability, particularly in low-inertia systems, more vulnerable grids, and weak points within robust networks.

Keywords: Synchronous condenser, power system stability, rotational inertia, reactive power support, RoCoF, frequency nadir.

Acknowledgements

We would like to express our sincere gratitude to everyone who has supported and guided us throughout the completion of this thesis during the final semester of our studies. We are especially grateful to ABB for the opportunity to conduct this thesis within their organisation. A special thanks to our supervisors, Gunnar Porsby and Carl Nilsson, whose support and continuous feedback have been invaluable throughout the project. We would also like to thank Erik Arnsten and Christian Payerl for their helpful discussions and technical inputs. Finally, we would also want to thank our academic supervisor and examiner at Chalmers, Massimo Bongiorno, for providing technical guidance and helping shape the direction of this thesis.

Anna Johansson & Amanda Schoberg, Gothenburg, June 2025

List of Acronyms

Below is the list of acronyms that have been used throughout this thesis listed in alphabetical order:

AVR	Automatic Voltage Regulator
BESS	Battery Energy Storage System
EMT	Electromagnetic Transients
GB	Great Britain
HVDC	High Voltage Direct Current
NESO	National Energy System Operator
OEL	Overexcitation Limiter
PSS	Power System Stabilizer
RES	Renewable Energy Source
RMS	Root Mean Square
RoCoF	Rate of Change of Frequency
SC	Synchronous Condenser
SCC	Short-Circuit Capacity
SVC	Static Var Compensator
UEL	Underexcitation Limiter

Nomenclature

Below is the nomenclature of parameters, and variables that have been used throughout this thesis.

δ	Rotor angle
dV/dQ	Relationship between voltage and reactive power
E_{kin}	Kinetic energy
f_{nadir}	Frequency nadir
f_0	Nominal frequency
H	Inertia constant
H_{sys}	Total system inertia
I_{sc}	Short-circuit current
J	Mass moment of inertia
RoCoF	Rate of change of frequency
S_b	Rated power of a synchronous machine
S_{sys}	System base power
SCC	Short-circuit capacity
Z_{th}	Thevenin impedance

Contents

1
Introduction

This chapter provides the overall background and motivation for this thesis, outlines its aim, and defines the scope and limitations. It also presents the research questions and ethical and environmental considerations.

1.1 Background

Integrating renewable energy sources (RESs) into power systems is a key strategy for reducing greenhouse gas emissions and addressing the significant CO_2 footprint of the energy sector. In recent years, this transition has progressed rapidly, driven by advancements in technology and policy support [1]. Consequently, power systems are undergoing a profound transformation, shifting from centralized power generation with large rotating machines to more decentralized systems where energy is produced from inverter-based energy sources closer to where it is consumed, as illustrated in Figure 1.1[2].

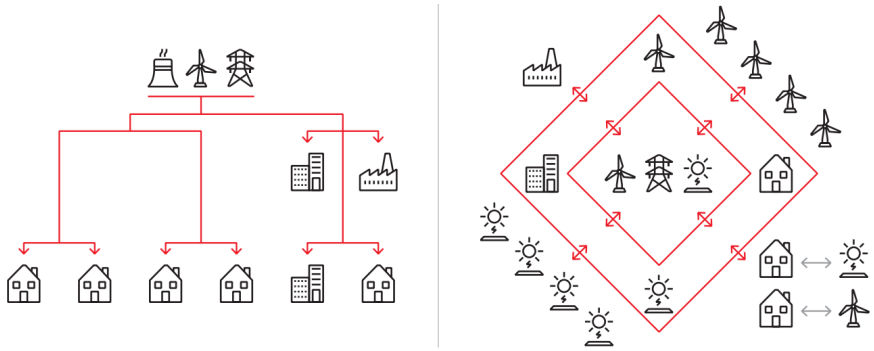

Figure 1.1: Comparison between traditional centralized power systems (left) and future decentralized grids (right), highlighting the shift toward distributed renewable energy sources. Reproduced with permission from ABB [3].

Unlike synchronous generators, most renewable energy sources are connected to the grid via power electronic converters, which do not inherently contribute to system inertia or short-circuit strength [4] [5]. As a result, power systems are experiencing reduced stability margins, particularly in regions with high renewable penetration or weak grid configurations. This shift raises challenges in maintaining frequency and voltage stability, especially during sudden disturbances such as load changes, short-circuit faults, or generation outages. These challenges highlight the growing

importance of reactive power compensation and the need for system inertia.

Synchronous condensers (SCs) offer a potential solution to these challenges. By providing rotational inertia, reactive power support, and short-circuit capacity, it can strengthen the power system by compensating for services that are reduced with the integration of RES [6][7]. The SC operates like a synchronous machine without a mechanical load and therefore does not provide any active power to the system [8]. SCs have been used since the 1930s, but have declined in use over the past 50 years since power electronics has become a more cost-effective solution for reactive power compensation. However, with the increasing integration of inverter-based energy sources, which contribute little to system inertia and short-circuit capacity, SCs have once again attracted attention as a valuable solution. This master's thesis is in collaboration with ABB and aims to explore how SCs can mitigate challenges faced in modern power systems with diverse grid topologies.

1.1.1 Previous Work

Some studies have investigated the role of SCs in supporting power system stability. One such study compares the dynamic performance of a conventional SC, a superconducting SC (SuperVAR), and a static var compensator (SVC) under various grid and fault conditions [9]. The authors conclude that SVCs performed better during faults causing small variations in voltage or faults in weaker grids due to their fast electronic switching and reactive power injection. During more severe disturbances, both SC models showed a better performance compared to the SVC, with shorter recovery times to nominal voltage. An explanation for this, presented in the paper, was that SCs can inject more reactive power as the voltage decreases due to the increasing difference in internal and terminal voltage, whereas the SVCs reactive power output is limited by the square of terminal voltage, meaning that during large voltage drops, the terminal voltage limits the reactive power injection to the grid.

A case study conducted on the British power system demonstrated that SCs can improve frequency stability by reducing the Rate of Change of Frequency (RoCoF) and increasing the tolerable generation loss following a disturbance [10]. The study showed that a 5 GVA SC with an inertia constant of 2 seconds reduced RoCoF from 0.116 Hz/s to 0.103 Hz/s, which corresponds to an improvement of approximately 12.6%. The SC also improved fault levels and short-circuit ratios, enhancing system strength and the operational security of HVDC connections.

According to a third study, the increased penetration of wind energy in power systems is leading to the replacement of conventional fossil fuel-based synchronous generators with variable-speed wind turbines [5]. Typically, they contribute with less fault current, resulting in a reduced system strength at the point of connection to the wind power plant, a factor that is critical for fault detection and recovery. Previous studies has demonstrated that this challenge can be addressed through the implementation of SCs or SVCs, as these devices contribute with additional fault current and help maintain system stability.

1.2 Aim

This master's thesis aims to evaluate the potential of synchronous condensers in modern power systems for enhancing grid stability. It focuses on how the synchronous condenser can contribute to reactive power support for voltage regulation and provide inertia for frequency stability.

1.3 Scope and Limitations

This study focuses on evaluating the performance of SCs in two contrasting power system configurations: a robust grid, representing a large and strongly interconnected system and an islanded grid, representing a smaller, islanded network with limited short-circuit capacity and inertia. These two cases are selected to reflect fundamentally different operating conditions and allow for the assessment of SC behaviour under varying system strengths. It is important to acknowledge that this thesis does not aim to conduct a detailed network analysis of specific power grids, but rather to use them as a framework for analysing the performance of the SC.

The thesis explores the capability of the SC to improve power system stability by supporting voltage regulation with reactive power and enhancing frequency stability through inertia contribution. These aspects are also analysed with comparisons between different deployment strategies, including centralized versus decentralized installations and the use of one large unit versus several smaller units. The analysis includes three SC unit ratings: 8 MVA, 67 MVA, and 200 MVA. The 8 MVA unit is evaluated in the islanded grid scenario, while the larger 67 MVA and 200 MVA units are assessed in the robust grid configuration.

The dynamic simulations and power system studies presented in this thesis are conducted using DIgSILENT PowerFactory, which is a widely used software platform for power system analysis [11]. While PowerFactory provides a robust environment for modelling and analysing complex power system dynamics, it is important to recognise that all simulation-based studies inherently involve certain assumptions and approximations.

1.4 Research Questions

This thesis aims to answer the following questions:

- How effectively does a SC contribute to voltage regulation and frequency support, and how does this performance differ between robust and islanded grid configurations during various disturbances?
- Where should the SC be deployed for optimal grid connection, and should it be implemented as one large unit or distributed as several smaller units?
- What are the limitations of the SCs?

1.5 Ethical and Environmental Considerations

The implementation of SCs in power systems raises some ethical and environmental considerations that it is important to acknowledge. These include both their potential to positively support environmental and societal goals as well as challenges that must be addressed to ensure responsible integration.

From an environmental perspective, the manufacturing of SCs requires large quantities of steel, copper, and insulating materials. Since these materials carry embedded emissions, the construction of SCs contributes to the overall environmental footprint. As SCs are large machines, installing them requires a considerable amount of space, especially when including necessary equipment like cooling systems. For this reason, SCs may be less suitable in settings where land availability or community impact is a concern.

By supporting renewable power generation, SCs can push the environmental impact of the power system in a positive direction. Investment in such technologies can help reduce the overall CO_2 emissions by replacing fossil fuel-based energy production and allowing more inverter-based sources into the system. Ensuring grid reliability is an ethical responsibility in itself, as power system instability can lead to widespread outages and compromised public safety. SCs can help enhance the stability and thus play a key role in maintaining important infrastructure and supporting the broader societal transition to renewable energy.

2

Power System Stability

The stability of power systems is a fundamental aspect of their reliable operation, ensuring that electrical grids can maintain equilibrium between generation and demand at all times. Power system stability refers to the ability of a power system to return to a steady operating condition following a disturbance, such as a short-circuit fault, loss of a generator or sudden changes in load [12].

Power system stability is typically divided into three main categories: rotor angle stability, frequency stability and voltage stability, as shown in Figure 2.1. Rotor angle stability concerns the ability of synchronous machines to remain in synchronism following disturbances, while frequency stability refers to the ability of the system to maintain its nominal frequency following imbalances between generation and demand [12]. Similarly, voltage stability ensures that voltage levels remain within acceptable limits at all buses and how well the system can restore equilibrium between generation and demand.

This chapter will continue by presenting the theoretical foundations of these stability phenomena and their implications for power system operation, beginning with a definition of basic power system operation in Section 2.1. It then continues with describing frequency stability and important frequency response metrics in Section 2.2, followed by voltage stability in 2.3. As this thesis will mainly focus on the frequency and voltage stability following the implementation of SCs, rotor angle stability is not discussed in detail.

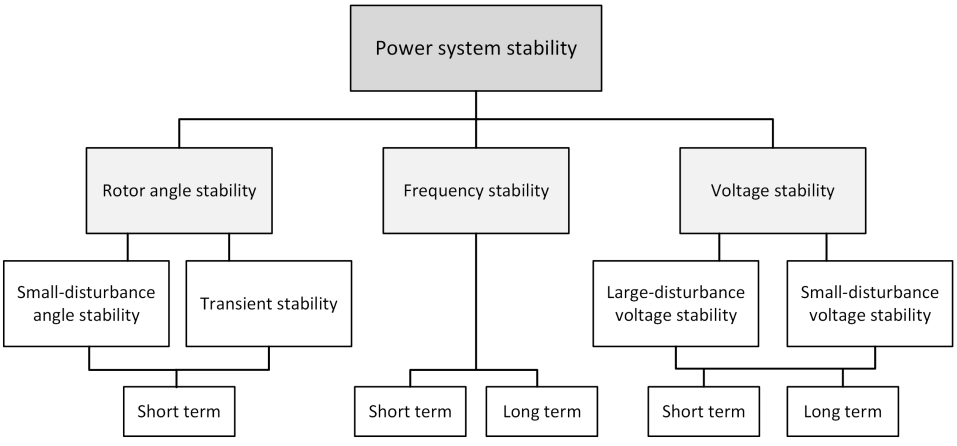

Figure 2.1: Power system stability classification. Redrawn and adapted from [12].

2.1 Basic Power System Operation

Understanding the fundamental operation of an AC transmission system requires knowledge of how electrical power is transferred from generation to load. There must always be a balance between the active power generated and the active power consumed in a system. Figure 2.2 shows an equivalent system diagram of a two-bus power system, consisting of a generation source, a transmission line and a load.

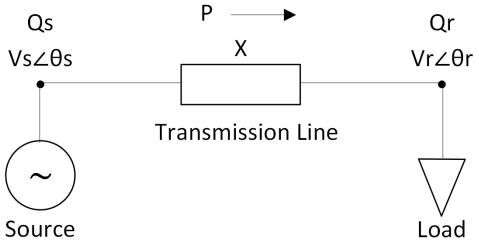

Figure 2.2: Equivalent system diagram of a two-bus power system, showing the active power flow, P.

The line reactance X is assumed to be purely inductive [8]. The relationship between voltage, transmission angle and line impedance determines the amount of power delivered through the transmission network [8]. This can be expressed mathematically using the power-angle equation, which describes the power flow and is defined as

$$P = \frac{V_s V_r}{X} sin(\theta_r - \theta_s) \tag{2.1}$$

where V_s and V_r are the voltage magnitudes at the sending and the receiving end, X is the line reactance and $\theta_r - \theta_s$ is the transmission angle, i.e., the angle difference between V_s and V_r [8]. This implies that maintaining appropriate voltage magnitudes and angle differences is important to ensure stable and efficient active power transfer.

While active power flow determines the transfer of real energy across the network, reactive power is equally important as it directly influences voltage levels and hence supports the stable operation of the system. Reactive power is naturally present in AC systems due to the inductive and capacitive characteristics of transmission lines, transformers and loads, which cause a phase difference between current and voltage [13][8]. However, this naturally occurring reactive power is not controlled and must be actively managed through compensation devices, such as SVCs or SCs. Active and reactive power are inherently linked, as the ability to transfer active power efficiently depends on maintaining appropriate voltage levels through reactive power control. Without sufficient reactive power, voltage stability may be compromised. The reactive power flow, given by

$$Q_s = \frac{V_r^2 - V_r V_s}{X} cos(\theta_r - \theta_s), \tag{2.2}$$

depends on the voltage levels at both ends of a transmission line and the line reactance. This illustrates how reactive power plays a direct role in regulating voltage magnitude. For example, an increase in reactive power demand leads to a voltage drop at the receiving end, especially over long distances [8].

2.1.1 Transmission and Distribution

In reality, an electrical power system is not a two-bus system but a large, complex network of interconnected generators, transmission lines, substations and loads that continuously balance supply and demand [8]. The network is typically divided into two main subsystems: the transmission system and the distribution system. The transmission system, often described as the backbone of the network, carries electricity at high voltages, usually above 230 kV [8]. To reach end users, the voltage is stepped down through transformers to lower levels in the distribution system, generally below 35 kV. However, these voltage levels can vary between countries or regions, and there is no universal standard that strictly defines the boundaries between transmission and distribution systems. In this study, both 400 kV and 21 kV are treated as transmission voltages, depending on the network model used. The 400 kV level represents a typical transmission voltage in a large, interconnected power system, while 21 kV is considered a transmission level within the small islanded grid model.

2.1.2 N-1 Contingency

To achieve reliability, the system must continue operating even if a component fails [14]. This is commonly evaluated using the N-1 contingency criterion, which means that the system must remain stable and operational following the loss of any single component in a network of N components.

2.2 Frequency Stability

Frequency stability describes the ability of a power system to maintain a stable frequency after experiencing a major disturbance that affects the balance between generation and demand [12]. If instability occurs, it can result in large frequency deviations, which can trigger the disconnection of generators or loads. In Europe, the nominal frequency is 50 Hz and is typically regulated within 49.5–50.5 Hz during normal operation, as specified in the grid code by Great Britain's National Energy System Operator (NESO) [15]. Frequencies beyond these limits are considered critical deviations, and it's important to restore the frequency toward the nominal condition to avoid instability. The system is expected to return to stable operation within the 47–52 Hz range after a disturbance. A drop to 47 Hz is especially serious, indicating a severe generation shortfall and bringing the system close to disconnection thresholds.

Frequency stability can be analysed using various metrics, two of the most significant

being the Rate of Change of Frequency (RoCoF) and frequency nadir. These metrics reflect how severely the system reacts to a disturbance and how well it recovers. Both are strongly influenced by the amount of rotational inertia in the system, which acts to slow down the frequency deviation following sudden power imbalances. The system's dynamic behaviour during frequency disturbances is described by the balance between input and output power. This relationship is captured mathematically by the swing equation.

2.2.1 Swing Equation

The swing equation models the dynamic behaviour of the rotor of a synchronous machine when there is an imbalance between mechanical input and electrical output power. This relationship explains how stored rotational energy resists sudden frequency deviations. Expressed in per unit form, the swing equation is defined as

$$\frac{2H}{\omega_s}\frac{d^2\delta}{dt^2} = P_m - P_e, \tag{2.3}$$

where H is the inertia constant, further explained in section 2.2.2, ω_s is the synchronous speed, δ is the rotor angle and P_m and P_e represent the mechanical and electrical power respectively [8]. The term $\frac{d^2\delta}{dt^2}$ describes the angular acceleration of the rotor, meaning that if the system is in a steady-state condition with no change in speed, the term equals zero. While the swing equation is often used in the context of rotor angle stability, it also provides a foundation for analysing frequency stability. Changes in rotor angle acceleration are directly related to changes in angular velocity and consequently, system frequency. By differentiating the relationship between rotor angle and angular speed, the swing equation can be reformulated in terms of frequency deviation as

$$\frac{2H_{sys}}{f_0}\frac{df}{dt} = P_{gen} - P_{load}, \tag{2.4}$$

where f_0 is the nominal frequency and P_{gen} and P_{load} is the active power generation and active power demand respectively [16]. This version of the equation describes the frequency behaviour as the result of a power imbalance, rather than the dynamic behaviour of a generator's rotor angle. This provides insight into frequency stability, making it more relevant for studies involving inertial response and frequency control, such as assessing the contribution of SCs in this study.

2.2.2 Inertia Constant

Rotational inertia plays a central role in power system stability, as it determines how strongly a synchronous machine resists changes in rotor speed following a disturbance. This inertia is provided by the rotating mass of the machine and is stored in the form of kinetic energy [17]. The rotational energy (or angular kinetic energy)

is defined as

$$E_{kin} = \frac{1}{2} J\omega^2, \tag{2.5}$$

where J represents the mass moment of inertia and ω is the rotational speed of the machine [18]. The kinetic energy is directly related to the inertia constant H of a synchronous machine. This is mathematically defined as

$$H = \frac{E_{kin}}{S_b} = \frac{1}{2} \frac{J\omega^2}{S_b}, \tag{2.6}$$

where S_b is the rated apparent power of the synchronous machine [16]. H, expressed in seconds, represents the time a synchronous machine can continuously supply its rated power using only its stored rotational kinetic energy and typically ranges between 2-10 s [8][18]. A higher value of H means that the rotating mass has more kinetic energy stored per unit of rated power, resulting in slower changes in rotor speed during a disturbance and thus slower frequency deviations. The inertia can also be defined in terms of equivalent system inertia, H_{sys}, as

$$H_{sys} = \frac{\sum_{i=1}^{N} S_{b_i} H_i}{S_{sys}}, \tag{2.7}$$

where S_{b_i} and H_i are the rated power and inertia constant of the ith machine in a system of N machines and S_{sys} is the total apparent power of the system [16].

2.2.3 Rate of Change of Frequency

The instantaneous rate of change of frequency, also known as RoCoF or df/dt, is measured at the time the instability occurs and represents how fast the frequency is changing over a short time interval [19], as shown in Figure 2.3. Measured in Hz/s, it describes how fast the frequency changes immediately after a disturbance and serves as a measure of the system's robustness. It is strongly related to the swing equation as stated in (2.4) and thus the total system inertia H_{sys}. The mathematical relationship of this can be expressed as

$$RoCoF = \frac{df}{dt} = \frac{\Delta P f_0}{2 H_{sys} S_{sys}}, \tag{2.8}$$

where ΔP is the power imbalance between generation and load [16]. A lower RoCoF indicates that the system experiences slower frequency deviations following a disturbance and hence a greater system robustness. This characteristic is typically associated with higher system inertia, which helps mitigate rapid frequency changes and allows more time for control systems to respond. According to NESO, the maximum allowed system RoCoF is $\pm$ 1 Hz/s [15].

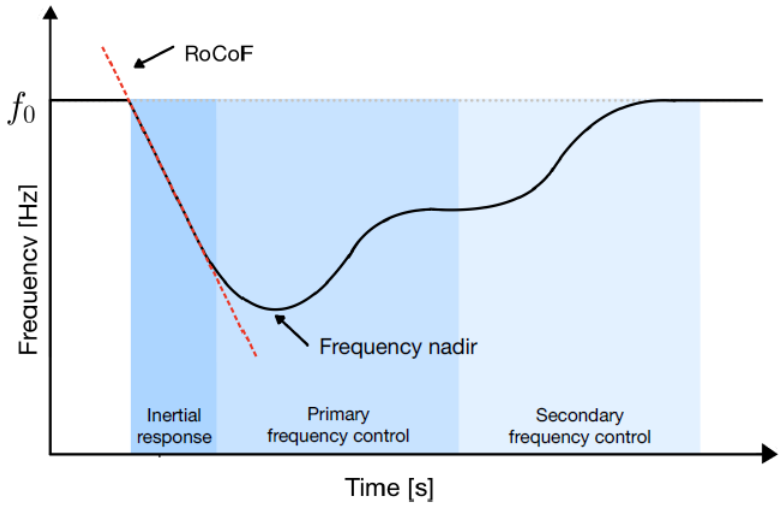

Figure 2.3: Frequency deviation following a disturbance, highlighting the inertial response area, RoCoF, and frequency nadir. Primary and secondary control actions are included for context.

2.2.4 Frequency Nadir

Frequency nadir, or f_{nadir}, refers to the lowest point of frequency reached after a disturbance, before the system begins to recover and the control mechanism can restore stability [20] and can be seen in Figure 2.3 above. A higher f_{nadir} indicates a more robust system able to limit frequency drops. It serves as a critical indicator of the power system's resilience. Although f_{nadir} is not always explicitly defined in the grid code, it is implicitly constrained by minimum frequency requirements following a disturbance, which is 49.5 Hz, according to NESO [15].

2.2.5 Primary and Secondary Frequency Control

The inertial response is an immediate physical reaction of rotating masses to a frequency deviation. It occurs instantly after the disturbance, without relying on any control action. Following the initial seconds, the primary frequency control activates, as seen in Figure 2.3 above. This control action mitigates further frequency decline and stabilizes the system by controlling the governors of the generators [21]. Subsequently, the secondary frequency control activates and the automatic generation control (AGC) starts to restore the frequency to its nominal value after 15 to 30 seconds [22]. These control systems regulate the active power output of generators to maintain frequency stability. Since synchronous condensers do not supply active power, they are not equipped with such control systems and they can therefore only contribute through their inertial contribution.

2.3 Voltage Stability

Voltage stability describes the power system's ability to maintain acceptable voltage levels across all buses during both normal operation and following disturbances [12]. It is typically divided into two categories: small-disturbance voltage stability and large-disturbance voltage stability [8][12]. This study will mainly focus on large disturbances, which concern the system's ability to maintain stable voltage levels following significant events such as short-circuit faults, sudden generation outages, or abrupt load changes. These disturbances initiate dynamic responses that challenge the system's voltage regulation and reactive power support. According to the grid code by NESO [15], voltage levels during normal operation must remain within the range of 0.95 to 1.05 p.u.

2.3.1 Short-circuit Capacity

In the literature, various approaches are used to define the strength of an AC power system. One of the most common is the short-circuit capacity (SCC), also referred to as short-circuit power. The value, expressed in MVA, represents the stiffness of the system voltage following variations in current [23]. It is defined as

$$SCC = \sqrt{3} \cdot V I_{sc} = \frac{V^2}{Z_{th}}. \tag{2.9}$$

where V is the nominal voltage prior to the fault, I_{sc} is the short-circuit current and Z_{th} is the equivalent Thevenin impedance. To determine the SCC of the system, a three-phase short-circuit fault is applied and the resulting current I_{sc} is measured. A higher SCC value indicates a more robust bus, characterized by a low impedance, and less sensitive to voltage variations [24]. In contrast, a lower SCC value reflects a weaker bus, which is more sensitive to voltage variations. In this study, SCC will serve as a metric for evaluating the optimal placement of SCs in the grid by identifying areas with low SCC.

2.3.2 QV-curve and dV/dQ

Another metric used for evaluating voltage stability in this study is dV/dQ sensitivity. It describes how sensitive the system's voltage is to changes in the reactive power injected or absorbed and can be measured at different buses in the system. The QV-curve, shown in Figure 2.4, is a graphical representation of the relationship between the change in reactive power ΔQ and voltage ΔV and can be defined as

$$\frac{dV}{dQ} \approx \frac{\Delta V}{\Delta Q}, \tag{2.10}$$

which indicates how much reactive power is required to achieve a given change in voltage [25]. In this study, reactive power is plotted on the vertical axis and voltage on the horizontal axis, meaning the slope of the curve represents dQ/dV. However, the sensitivity metric of interest is dV/dQ, which is the inverse of the curve's slope. The point where dV/dQ (and dQ/dV) equals zero indicates the voltage stability

limit and represents the minimum voltage the bus can withstand before entering an unstable operating condition, as seen in the figure. A higher dV/dQ value implies that the bus voltage is more sensitive to changes in reactive power, meaning it requires a smaller amount of reactive power to cause a voltage change compared to a bus with a lower dV/dQ value.

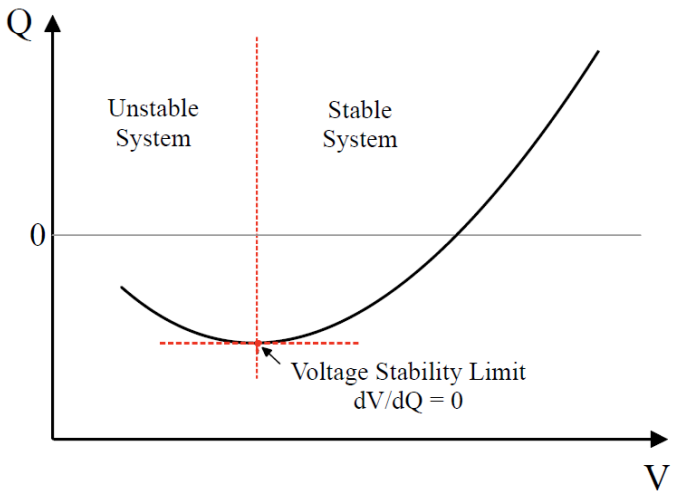

Figure 2.4: QV-curve showing the stable and unstable regions together with the voltage stability limit where dV/dQ = 0.

2.4 Summary of Stability Evaluation Metrics

The stability and performance metrics used in this thesis have been introduced and described throughout this chapter. These values are based on the grid code requirements from NESO [15]. Table 2.1 summarizes the evaluation metrics used in this analysis. The NESO grid code specifies ride-through durations of up to 90 minutes, depending on the severity of the disturbance. However, this thesis limits the analysis to the first 60 seconds following a disturbance, as this time frame captures the critical dynamic response phase of the evaluated faults. While long-term capability lies outside the scope of this study, the evaluation metrics are still used to assess the results against the relevant operational limits specified in the grid code.

Table 2.1: Summary of normal operational limits and evaluation metrics, as defined in [15].

Operating Condition	Metric	Symbol	Reference Value
Normal operation	Frequency range	f	49.5 - 50.5 Hz
	Voltage range	V	0.95 - 1.05 p.u.
During disturbance	Rate of change of frequency	RoCoF	± 1 Hz/s
	Frequency nadir	f_{nadir}	≤ 49.5 Hz

3
Synchronous Condenser

Synchronous condensers (SCs) are a type of active shunt compensator that has been used since the 1930s to control reactive power in power systems, before power electronics became widely used for such compensation. [26] [8]. As the amount of RES increases rapidly in today's power systems, SCs have attracted new attention as they provide both voltage and frequency support through dynamic reactive power control and their rotational inertia. Another key benefit is their ability to increase the system's SCC, thereby enhancing stability during faults [8]. Compared to other types of shunt compensators, SCs produce reactive power independently of the system voltage thanks to their internal voltage source, which allows them to operate effectively even under severe voltage drops.

This chapter outlines the fundamental working principle and internal structure of the SC. Furthermore, it describes how SCs contribute to frequency regulation by releasing kinetic energy stored in its rotational mass, thereby supporting the inertial response during frequency disturbances. Lastly, this chapter discusses the process of reactive power compensation, highlighting the operation of the control system responsible for maintaining voltage stability.

3.1 Working Principle

The SCs operates similarly to a synchronous motor or generator, however it is not connected to a mechanical load and therefore does not produce mechanical power [8]. Instead, its primary function is to supply or absorb reactive power to support voltage stability in the grid and to contribute to system inertia. It only draws a small active power component from the grid to compensate for the internal losses in the machine [27].

A synchronous machine consists primarily of two components, the armature and the field winding [8]. The armature windings are typically mounted on the stator of the machine, while the field windings are placed on the rotor. A direct current, supplied via brushless or static excitation, flows through the field windings of the machine. This excitation current produces a magnetic field, and as the rotor rotates, this induces an AC voltage in the armature windings. The rotor is synchronized with the electrical grid and rotates at grid frequency. By adjusting the excitation current, the machine's internal voltage can be controlled. The direction and magnitude of reactive power exchange with the grid are determined by the difference between

this internal voltage and the grid voltage, enabling the machine to supply or absorb reactive power accordingly. This is automatically managed via its control system, further described in Section 3.3.

As mentioned, the SC contributes to the system's SCC by contributing with short-circuit current, I_{sc}, following a disturbance. When a fault occurs, such as a short-circuit, the system voltage drops and currents are induced in the rotor of the machine [8]. The currents that decay the fastest during such an event are described by the subtransient parameters. When analysing the short-circuit contribution of the SC, it is essential to consider both its internal characteristics and the external system parameters, as they both affect the immediate response from the SC. The sub-transient reactance, X''_d, and the transformer leakage impedance, X_t, are two critical parameters in this analysis [27]. Low reactance values of X''_d and X_t are beneficial for improving system strength, as they lead to a higher SCC by allowing greater I_{sc}. Optimizing these reactances can therefore significantly influence the performance and efficiency of the SC [28]. A simplified single-line diagram of the SC, including these reactances, is shown in Figure 3.1.

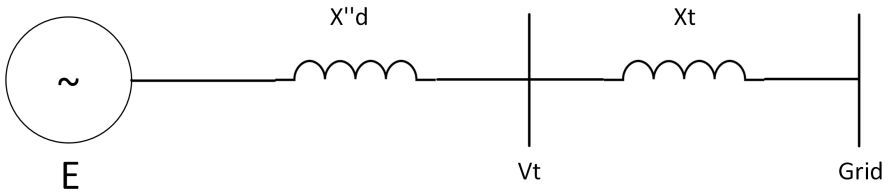

Figure 3.1: Single-line diagram of SC where X''_d is the sub-transient impedance, V_t is the terminal voltage and X_t is the transformer impedance.

3.2 Frequency Support

The frequency support from an SC is provided by the rotational inertia of the machine. As a result, the SC only contributes to the inertial response during the first seconds following a disturbance and does not take part in primary or secondary frequency control. To further enhance its frequency support, the machine can be combined with a flywheel, which is a mechanical device used for providing additional rotational energy in the SC application [6]. The additional rotational mass increases the machine's inertia constant, H, and consequently the total system inertia, H_{sys}. During power fluctuations in the system, the SC and the attached flywheel release the kinetic energy stored in their combined rotational mass to help limit the frequency deviation [8][29]. This change positively influences RoCoF and f_{nadir}.

3.3 Voltage and Reactive Power Control

In combination with a voltage regulator to control its excitation, the SC can either inject or absorb reactive power to help stabilize the terminal voltage across varying grid conditions [8]. To protect the machine from damage during extreme operating conditions, the SC can be equipped with excitation limiters to ensure that the excitation is within safe limits. The following section outlines the process of reactive power compensation, detailing how the excitation system, in combination with the Automatic Voltage Regulator (AVR), voltage transducers, and protective limiters, works together to maintain optimal and safe operation and performance. A simplified overview of the SCs control system can be seen in Figure 3.2.

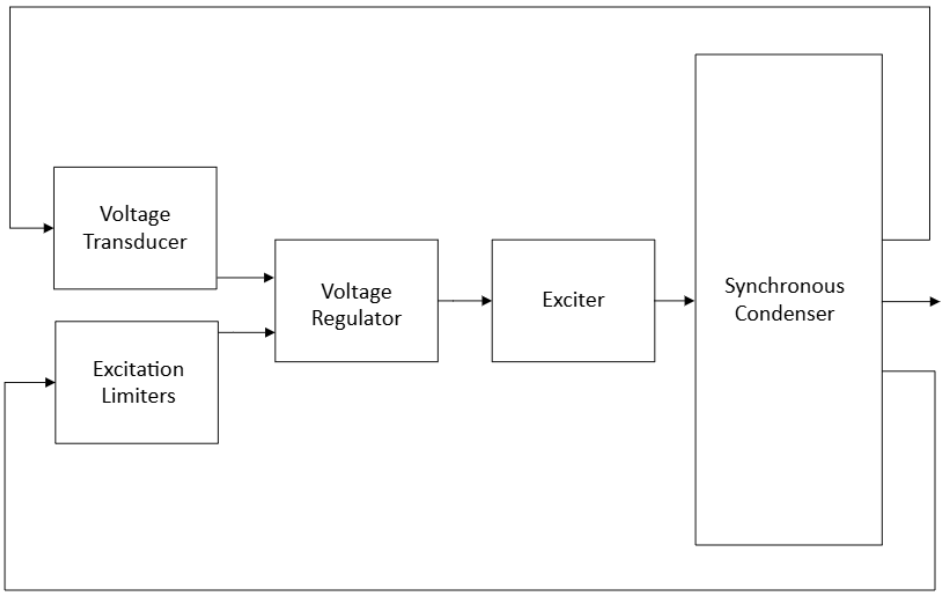

Figure 3.2: Simplified representation of the control system

3.3.1 Excitation System and AVR

The excitation system, together with the Automatic Voltage Regulator (AVR), controls and regulates the operation of a synchronous machine [8]. From a power system perspective, the excitation system ensures that the machine responds effectively to voltage variations. The terminal voltage is continuously monitored by the voltage transducer, which produces a DC signal for further processing [8]. The DC signal is compared with a reference voltage, and based on the resulting voltage deviation, the excitation current is adjusted to regulate the reactive power exchange. If the system voltage drops, the excitation current increases to supply more reactive power. Conversely, if the voltage rises, the excitation current is reduced, causing the SC to absorb reactive power. This enables the SC to dynamically regulate reactive power and support voltage stability. Following a fault, there is typically a delay of a few hundred milliseconds before the AVR responds. This means that if the fault duration is shorter, the AVR may not have enough time to react. As a result, the SC can

only respond to the fault through its immediate short-circuit current contribution, while the AVR begins to regulate after the fault has been cleared.

3.3.2 Underexcitation and Overexcitation Limiters

In the excitation system of a machine, there are protective controls that set boundaries for the excitation of the SC to ensure that the excitation is within the operating limits of the machine to avoid damage [8]. These limiters are commonly referred to as underexcitation limiters (UEL) and overexcitation limiters (OEL). When the terminal voltage drops significantly, it can result in a high current flowing in the field windings of the synchronous machine. If this current is supplied during an extended period of time, the OEL prevents the machine from overheating by limiting the current [8]. In opposite, the UEL steps in to ensure that the decrease in excitation of the machine does not cause steady-state instability or excessive thermal stress in the end part of the stator core. A capability diagram that illustrates UEL and OEL can be seen in Figure 3.3. However, as can be seen in the figure, the SC only operates by controlling reactive power, and hence the active power is only relevant for synchronous generators and motors.

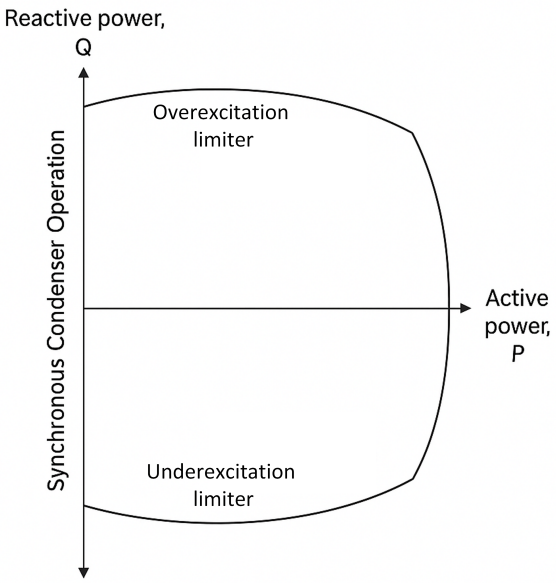

Figure 3.3: Capability diagram of a synchronous machine, showing the under- and overexcitation limitation in the control system.

4
Synchronous Condenser Modelling

This chapter presents the modelling process and implementation of the three differently rated SCs, as well as the development and implementation of their respective control systems. Additionally, it includes a verification of the dynamic models under operating conditions similar to those expected in the actual application, essential to ensure that the models perform as intended before proceeding to more complex simulation environments.

4.1 Modelling the Synchronous Condenser

Three different sizes of SCs, rated 8 MVA, 67 MVA and 200 MVA were modelled in PowerFactory. The models were developed based on detailed machine parameters and control system settings provided by ABB. The SCs were modelled as synchronous machines without any active power contribution. Both the 67 MVA and 200 MVA SCs were equipped with flywheels, whereas the 8 MVA unit used in this study was not. The additional inertial contribution from the flywheel was incorporated via an increased inertia constant, eliminating the need for separate modelling. The rated power, voltage, and inertia constants for each unit are presented in Table 4.1.

Table 4.1: Important modelling parameters for all SCs used in this study.

SC	**8 MVA**	**67 MVA**	**200 MVA**
Rated power [MVA]	8	67	200
Rated voltage [kV]	10.5	13.8	13.8
Inertia constant [s]	2.306	7.046	8.024

4.1.1 Control System

In addition to modelling the SCs physical parameters, a representation of the machine's control system was required. The excitation system and AVR for the 8 and 67 MVA machines were based on the IEEE standard model AC11C, as defined in IEEE Std. 421.5-2016 Recommended Practice for Excitation System Models for Power System Stability Studies [30]. Modelling of the control system also required an overexcitation and underexcitation limiter, IEEE OEL2C and UEL2C. In addition, the IEEE voltage transducer and current compensator were added to the

control system. The input parameters to all functions in the control system were modified to suit the different sizes of the condensers. The control system for the 200 MVA unit was simplified by assuming a static excitation system, due to limitations of the parameter data. As a result, a simpler excitation model, ST1A, from the same IEEE standard was used. For this simplified approach, the implementation of overexcitation and underexcitation limiters was excluded.

4.1.2 Step-up Transformer

The voltage ratings of the units assessed in this study are 10.5 kV and 13.8 kV, as shown in Table 4.1 above. Depending on the voltage requirements, a two-stage transformer configuration was used, consisting of a step-up transformer in series with the SC to match the machine's terminal voltage with the grid voltage. By connecting the SCs in parallel to a common bus, the need for individual transformers for each unit was eliminated. However, the transformer rating must be appropriately selected to allow maximum reactive power compensation from the SC. Input data is based on [31] and presented in Table 4.2. The modelling was simplified by allowing for potentially high currents through the transformer due to the ratio between power and voltage. This simplification was considered acceptable, as the aim of the study is to analyse the behaviour of SC rather than to optimise the design of the transformer.

Table 4.2: Modelling parameters for the transformers used in this study [31].

Transformer [kV/kV]	**33/400**	**13.8/33**	**10.5/21**
Configuration [-]	Y/Yn	Y/Yn	D/Yn
Rated power [MVA]	600	400	50
Series resistance [p.u]	0.002	0.002	0.002
Series reactance [p.u]	0.1	0.1	0.1

4.2 Model Verification

To verify that the SCs and their respective control units were correctly modelled in PowerFactory, several pre-study simulations were performed. The test environment was modelled only with transformers and an SC connected to an infinite bus, isolating the system from influences from other system components. This was done for each SC unit. The infinite bus was represented by a voltage source behind a series impedance, defined via its SCC and X/R ratio. The test setup was used to assess the dynamic response from the SC and confirm proper operation of the AVR and the exciter. Data for the infinite bus was based on results from the short-circuit analysis, described in Chapter 5.

By varying the SCC of the external grid from 50 MVA to 13000 MVA, different system strength scenarios were simulated, representing both islanded and robust

grids. The 8 MVA unit was tuned for operation under lower SCC values, while the 67 MVA and 200 MVA units were tuned for higher SCC values. This allowed the control system for each SC unit to be adjusted to reflect expected behaviour under realistic grid conditions.

To evaluate the system's voltage regulation response, a step change in the AVR reference voltage, V_{ref}, was applied, increasing it from 1.0 to 1.025 p.u. as part of the verification tests. All SC models reached 90% of the new terminal voltage step change within approximately 400 ms as seen in Figure 4.1. Variations in voltage behaviour were primarily observed following the initial rise phase, particularly in terms of overshoot and steady-state voltage. These differences can be explained due to variations in control parameters, such as proportional and integral gains.

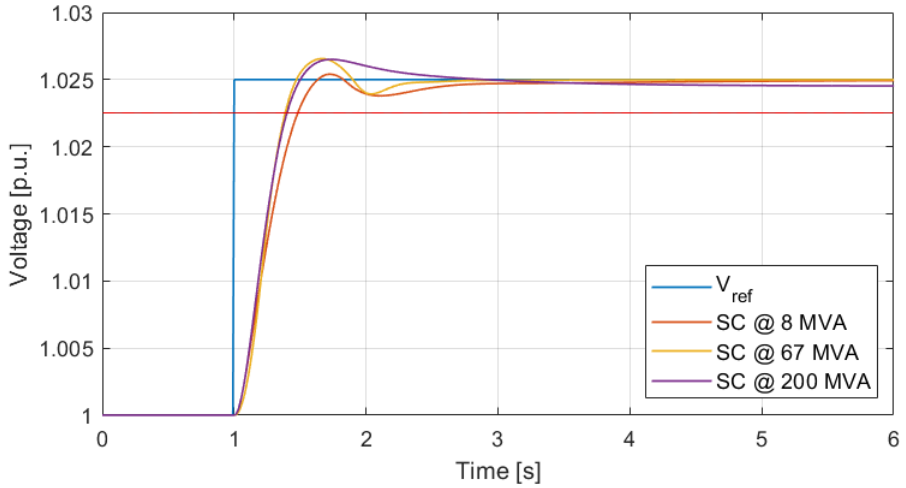

Figure 4.1: Voltage response following a step change increase in the reference voltage, V_{ref} for synchronous condensers (SCs) of 8, 67, and 200 MVA capacity. The red line indicates 90% of increase in V_{ref}.

4.3 Limitations

It is important to note that the constructed representation of the SC is based on approximations and assumptions, and can be considered an idealised model. The simulation does not capture all real-world physical phenomena occurring in the machine during operation, such as heating, material degradation, or environmental influences, although some of these effects are estimated through parametrisation. As a result, its behaviour in the simulation may differ from its real-world performance. Furthermore, the control system is modelled in a simplified way, which may not fully reflect the system's dynamic response or protection mechanisms.

As previously mentioned, when verifying the response of the SC in an isolated grid, there are no other components or control systems for it to interact with. However, when connected to a more complex grid model, the SCs response is affected by the presence of multiple generators, loads, transmission lines, compensators, and their

respective control systems. As a result, its behaviour is affected by the requirement to operate in coordination with all these elements.

5

Robust Grid Model and Scenario Description

This study utilizes two pre-existing power system models to represent a large interconnected grid and a small isolated grid. These models are not analysed in terms of real-world performance, but instead serve as platforms to explore how SC behave in power systems with two different system strengths. This chapter focuses on the larger grid model based on the Great Britain transmission system, and is hereafter referred to as the *robust grid model*, due to its high SCC. The *islanded grid model* is described in Chapter 6.

The robust grid model is based on the GB 36-bus model and is a publicly available, reduced equivalent of the National Electricity Transmission System (NETS) of Great Britain. It is developed in DIgSILENT PowerFactory by NESO and based on data from 2013 [32]. This chapter outlines the structure of the model, including the modifications made to adapt it for this study. In addition, it describes the simulated fault scenarios and the deployment strategies used for the placement of SCs.

5.1 Base Model and Alterations

The robust grid model includes 36 zones, each represented by one bus and interconnected to the remaining zones via transmission lines. A full diagram of the model from PowerFactory is presented in Figure 5.1. Each bus contains one load and multiple generators. Wind, marine, and HVDC sources are modelled as static generators. Remaining generators such as nuclear, oil, hydro, pumped hydro, biomass, coal and other types of generation are modelled as dynamic generators equipped with both an AVR and a governor. In the base model without alterations, all coal generators were out of service, a setting that was kept throughout the study. In several zones, additional reactive power compensation is provided by a Static Var Compensator (SVC) or other Static Var Systems (SVS). Due to limitations in the dynamic modelling of SVCs and SVS, numerical stability issues were observed during Electromagnetic Transient (EMT) simulations. As a result, these were replaced with fixed capacitors and reactors, sized according to their reactive power contributions from power flow analysis. Accurately modelling SVCs for EMT simulations would require modifying their control systems, which was considered outside the scope of this study.

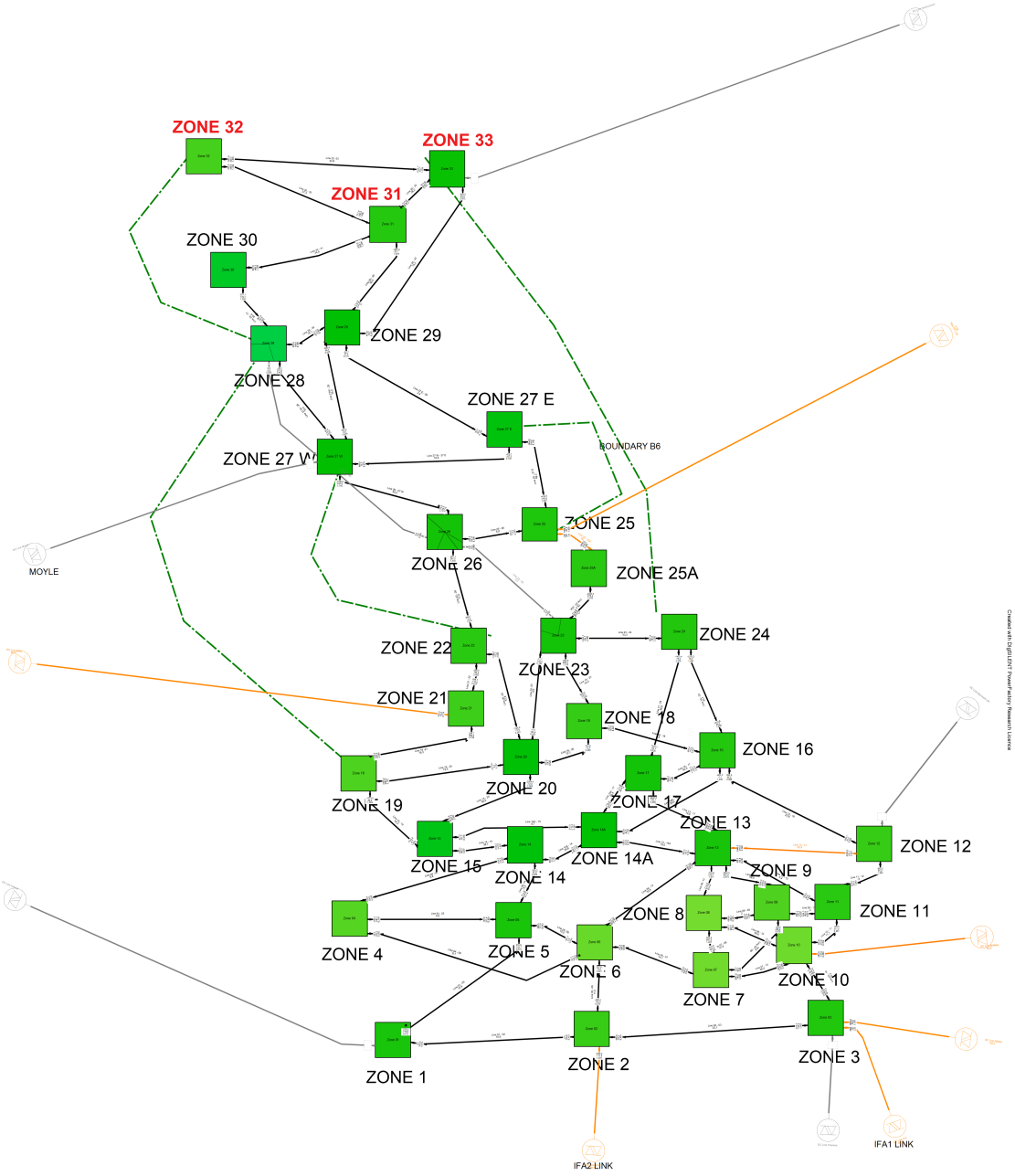

Figure 5.1: The GB-36 bus model [32] from PowerFactory displaying all the zones in the network. The zones of interest for this study are marked in red.

An initial three-phase short-circuit analysis was conducted in the model, confirming the robustness as SCC values exceeding 20 000 MVA were observed in the system. As a consequence, some adjustments were made. To simulate a system with high renewable penetration, nuclear generation from all active units was reduced by 20%, corresponding to approximately 2000 MW. To maintain system balance, this reduction was replaced by an increase in wind generation with corresponding output. This additional wind power was distributed across multiple zones to reflect realistic geographical distribution and to ensure that all turbines operated within their

ratings. With these modifications implemented, and all remaining generators and loads operating as expected, this is referred to as the *base case*.

To identify weak areas in the new base case where the installation of an SC could enhance system stability and performance, another three-phase short-circuit analysis was performed at the 400 kV bus in each zone. This analysis provided the different SCCs in each area and served as a key indicator of system strength. Buses with low SCC were identified as potential weak points, as they are more sensitive to voltage variations. The results of this analysis were used to investigate the strategic placement of SC units, ensuring they are located where they can be beneficial for voltage regulation. The results of the short-circuit analysis for the zone with the lowest SCC, along with its neighbouring zones, are presented in Table 5.1. Complete results for all zones, including load flow voltage values for the respective buses, are provided in Appendix **??**.

Table 5.1: SCC of the three neighbouring zones with the lowest SCC. A full list of all zones SCC can be found in Appendix A (Table A.1).

Zone	**Nom. Voltage** [kV]	**SCC** [MVA]
31	400	10356
32	400	9245
33	400	9252

5.1.1 Zone 32

Based on the results from the short-circuit analysis, Zone 32 was chosen for further analysis as it was identified to have the lowest SCC at 9245 MVA. The generation is distributed between gas, hydro, pumped hydro, marine, wind, and other types of generation. A single-line diagram of Zone 32 and the ratings for all the generators can be seen in Figure 5.2. As can be seen in the figure, the majority of generation comes from wind, hydro, and pumped hydro and hence, this is a good representation of a zone with high penetration of RES. Additionally, one load and two transmission lines, interconnecting Zone 32 with Zone 31 and 33, are connected to the 400kV bus.

To investigate system stability under stressed conditions, a set of N-1 contingencies was simulated for Zone 32 to reflect realistically weakened operating scenarios. This included the disconnection of a gas turbine, a pumped hydro unit, and an outage of the transmission line connecting Zone 32 to Zone 33. The two generators were selected due to their differing generation capacities, while the transmission line outage was considered interesting as it reduced support from neighbouring zones. Each contingency was simulated over the full simulation period during Scenario 1, further described in Section 5.2. Their respective impacts were compared to identify the most critical N-1 event.

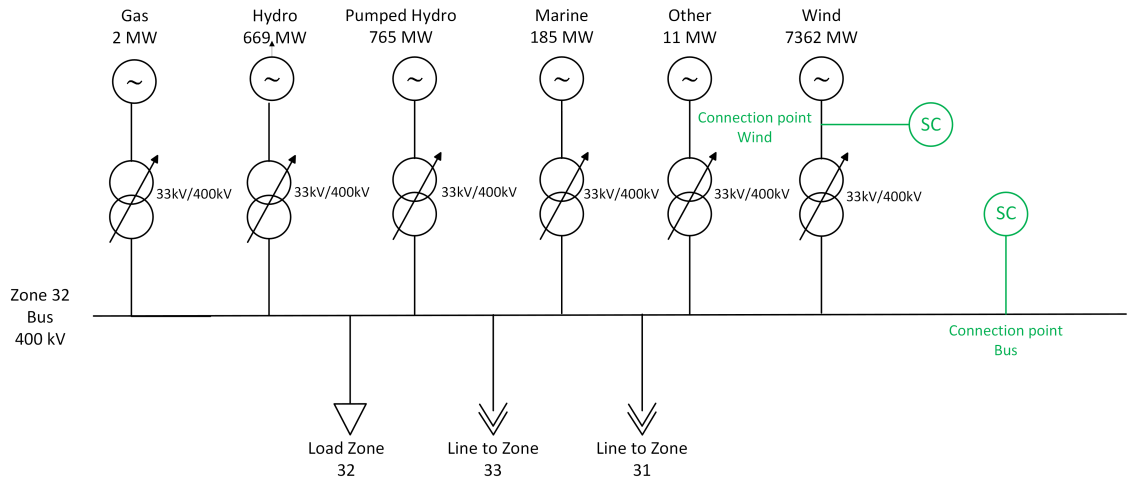

Figure 5.2: Single-line diagram of Zone 32, illustrating generators, loads, transmission lines connecting to neighbouring zones, and proposed SC implementations.

5.2 Fault Scenario Description

Three fault scenarios were simulated using the robust grid model to evaluate the performance of the SC under typical grid disturbances. These included a three-phase short-circuit on a transmission line, a similar fault on a second transmission line, and a generation loss at a hydro power plant. The scenarios were selected to assess the SCs contribution to voltage and frequency stability. Each event was analysed under two operating conditions, the base case and the N-1 base. EMT simulations were used for short-circuit events to accurately capture fast dynamics, while RMS simulations were sufficient for scenarios involving generation loss, due to slower system dynamics and analysis over a longer time period. The following section outlines each of the simulated disturbances in detail.

1. Three-phase Short-circuit Event on Transmission Line Zone 31-32: The first scenario involved a three-phase fault with zero impedance at the midpoint of the transmission line between Zone 32 and Zone 31. The fault, with a duration of 50 ms, was simulated to assess the SCs response to a fault in the nearby area, causing a severe voltage dip.

2. Three-phase Short-circuit Event on Transmission Line Zone 29-31: The second scenario simulated a similar three-phase fault with zero fault impedance on a second transmission line, with a duration of 50 ms. This event was designed to evaluate the response of the SC to a fault occurring further away, introducing more impedance between Zone 32 and the fault location, and consequently resulting in a milder voltage dip.

3. Loss of Generation at Hydro Power Plant: The third scenario simulated a generation loss of 0.85 p.u. at the hydro power plant in Zone 32, represented by a

sudden reduction in mechanical torque in the synchronous machine after 1 second. This scenario aimed to assess the SCs ability to support system inertia and improve the RoCoF and the f_{nadir}.

5.3 Synchronous Condenser Placement

To evaluate the optimal deployment strategy for SCs, several connection strategies were evaluated. Each configuration was tested using two levels of total compensation of approximately 200 MVA and 400 MVA. These were achieved by combining three or six 67 MVA units, or one or two 200 MVA units. This enabled a direct comparison of system performance between configurations using different SC ratings, while maintaining the same total capacity. Due to the high system strength, compensating with fewer SCs was not considered relevant. The connection of the SC to either the bus or the wind bus in Zone 32 is illustrated in Figure 5.2.

Centralized - Connected to Bus in Zone 32
In the centralized configuration, the SCs were connected to the 400 kV bus in Zone 32. This setup served as the reference case for evaluating centralized deployment, representing a typical approach where support is concentrated in a single, strategically selected location with lower SCC, here represented by the bus in Zone 32 with SCC of 9245 MVA.

Decentralized - Connected to Buses in Zone 31, 32 & 33
For the decentralized configuration, 67 MVA SCs were distributed equally in neighbouring Zone 31, Zone 32, and Zone 33, each connected to its respective 400 kV bus. The total compensation provided matched that of the centralized setup of either 200 MVA or 400 MVA, allowing for direct comparison of performance. Deployment in more distant zones or areas with high SCC was not considered relevant, due to limited compensation contribution from SCs in such areas.

Local - Connected to Wind Bus in Zone 32
The SC was connected to the bus of the wind power plant in Zone 32, allowing for analysis of its performance at a lower voltage level of 33 kV and in a part of the zone characterised by lower SCC. This deployment strategy was particularly relevant for evaluating the SCs ability to enhance stability in weaker areas of the grid.

6

Islanded Grid Model and Scenario Description

In contrast to the large-scale interconnected power grid discussed in the previous chapter, this chapter focuses on a small islanded power system, which is more vulnerable to fluctuations and disturbances due to its limited size and low SCC. This model is designed to reflect the characteristics of a low-inertia, weaker grid system with a majority of RES production, making it particularly relevant for studying the implementation of SC. This system will henceforth be referred to as the *islanded grid model*.

The grid model used to represent a smaller, isolated power system is based on a model of the southernmost island of the Faroe Islands. The original model was developed by Helma Tróndheim as part of her PhD research [33]. Since the objective of this thesis is not to analyse a specific grid, the model has been altered and changed to represent a general islanded grid, with areas and busbars renamed to reflect this generalized approach. The main components and configuration of the model are described in this section, along with the specific alterations made for this thesis.

6.1 Base Model and Alterations

The model is divided into five areas: a central area (Bus 1), an oil area (Bus 2), a hydro area (Bus 3), a load area (Bus 4) and a wind farm (Bus 5.1-5.7), as seen in Figure 6.1. The central area forms the core of the grid structure, serving as the connection point between the wind farm and the other areas. As indicated by their names, this islanded system includes three main generation sources: two hydropower generators, one oil power plant, and a wind farm represented by seven static generators. The hydro and oil generators are modelled as dynamic generators with appropriate control systems, including governors and AVRs configured for each generation type. The two hydropower plants, HYDRO G1 and HYDRO G2, are rated at 1 MW and 2 MW, respectively. The oil power plant, OIL G1, is rated at 4.1 MW. The wind farm consists of seven static wind generators (WIND T1–T7), each rated at 0.9 MW, with a static dispatch of 0.4 MW per generator under normal operating conditions to represent moderate wind conditions. The load area, as well as the oil and hydro areas, are designed as substations with loads connected to the buses. The loads are modelled as static PQ loads that represent smaller distribution networks. An important detail not shown in the figure is that both the oil area

and the load area contain two voltage levels: a 10.5 kV bus where the generators and loads are connected, and a 21 kV bus used for transmission. These buses are interconnected via transformers within each area. The hydro area only consists of one bus operating at 10.5 kV. Lastly, all transmission elements in the system are modelled as underground cables. A summary of the load flow values, generator ratings and all bus voltages and types of the altered islanded grid model is presented in Appendix B.

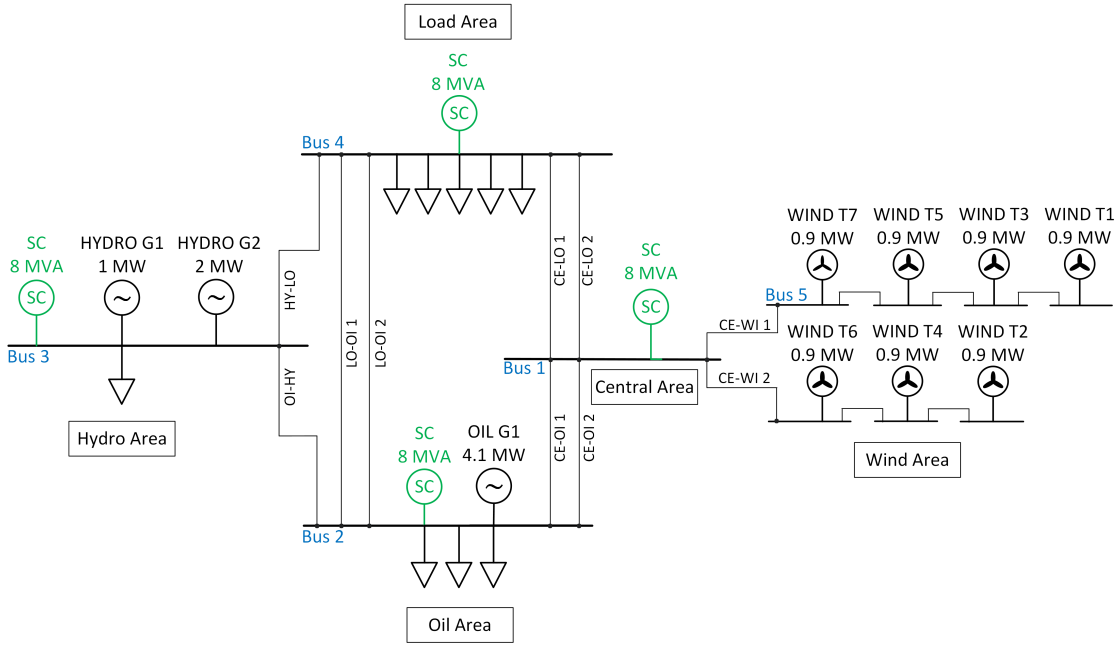

Figure 6.1: Simplified diagram of the islanded grid model. The SCs marked in green indicate the bus locations used in the different test configurations of this study.

The original grid model included an SC rated at 8 MVA, connected at Bus 1 in the central area. For this study, the unit was disconnected to enable a clearer evaluation of the SC's impact. This adjustment resulted in slightly reduced load flow voltage levels across the grid, with the lowest bus voltage reaching approximately 0.961 p.u. This value, while somewhat low, remains within the grid code's normal operating range of 0.95–1.05 p.u. and highlights the underlying need for reactive power support in the system. The voltage level was deemed acceptable, as it allows for a meaningful comparison between cases with and without SC support without compromising system stability. The analysis therefore begins from a base case without any SCs and focuses on assessing the effects of incrementally adding one or more units in different locations.

A Battery Energy Storage System (BESS) present in the original model was excluded in this study. The decision to disconnect the BESS was made to ensure the model's stability. The integration of the BESS would have required extensive modifications to the underlying simulation scripts, which were beyond the scope of this thesis. Additionally, parts of the original model's relay protection system

were deactivated for similar reasons. Since the primary objective of this thesis is to evaluate how SCs can enhance power grid stability in terms of frequency and voltage support, retaining the full original relay configuration was not essential for the intended analyses.

Similarly to the robust grid model, a short-circuit analysis was performed to evaluate optimal weak points for the connection of the SC. This is presented in Table 6.1. As shown in the table, the differences in SCC between the buses are relatively small. Therefore, the conclusion was that it would be interesting to evaluate the performance of the SC at multiple bus locations to explore whether these minor variations in SCC have a noticeable impact on system stability.

Table 6.1: SCC values of selected buses in the islanded grid model. A complete list of all bus SCC values is provided in Appendix B (Table B.2).

Area/bus	**Nom. Voltage** [kV]	**SCC** [MVA]
Central area/Bus 1	21	45.01
Oil area/Bus 2	21	46.61
Hydro area/Bus 3	10.5	39.73
Load area/Bus 4	21	44.85
Wind area/Bus 5	21	44.25

6.2 Fault Scenario Descriptions

The selected scenarios were designed to evaluate the performance of SCs in an islanded grid under typical severe disturbances affecting voltage and frequency stability. Due to limitations in the dynamic model of the islanded grid model, only RMS simulations were conducted. To evaluate the performance, three fault scenarios were chosen: a three-phase short-circuit trip on cable LO-OI 1, a generation loss scenario of HYDRO 1 and a load rejection scenario of a load in the oil area. These scenarios were chosen to investigate both the voltage and frequency behaviour, both pre- and post-connecting the SCs. The scenarios are:

1. Three-phase short-circuit fault on LO-OI 1: The first scenario involved simulating a three-phase short-circuit fault on one of the two parallel underground cables connecting the load area and oil area. The fault had 1 Ω fault impedance was located at the midpoint of the 18 km cable, and lasted for 150 ms. While the probability of a three-phase fault occurring on a cable is relatively low compared to overhead lines, this scenario was chosen to evaluate the system's dynamic voltage response.

2. Generation loss of HYDRO G1: The second scenario simulated the loss of generation from HYDRO G1, located at Bus 3. The generation loss was mod-

elled as a sudden decrease of 0.8 p.u. torque, representing a significant reduction in power input to the system. This fault was included to study the system's frequency behaviour.

3. Loss of Load: The third scenario involved a sudden reduction of 30% of a load in the oil area. This reduced the total system load by 3.8% in both active and reactive power, simulating a decrease in demand and testing the system's ability to maintain frequency stability under load-shedding conditions.

6.3 Synchronous Condenser Placement

The SC placements used in this study are illustrated in green in Figure 6.1. Across all three fault scenarios, 8 MVA SCs were added incrementally at different buses to evaluate how placement influences system performance and how many SCs are needed for sufficient improvement. For each case, multiple simulations were conducted, with one SC added at a time at the locations shown in the figure.

7

Simulations Results from Robust Grid Model

This chapter presents the simulation results obtained from the robust grid model developed in PowerFactory. Three fault scenarios were simulated to evaluate the system's voltage and frequency responses under different types of disturbances, both before and after the implementation of 67 MVA and 200 MVA SCs. The fault scenarios tested in this grid model include:

- **Scenario 1:** A three-phase short-circuit on the transmission line connecting Zone 31 and 32
- **Scenario 2:** A three-phase short-circuit on the transmission line connecting Zone 29 and 31
- **Scenario 3:** A loss of generation at the hydro power plant in Zone 32, resulting in a mechanical torque reduction of 0.85 p.u.

To accurately capture the system's fast dynamic behaviour during short-circuit events for voltage analysis, EMT simulations were applied. For frequency-related studies, when observing the response over longer time periods, RMS simulations were used as they are more suitable for such analysis. Both the base case and the most critical N-1 contingency, as further discussed under Scenario 1, were simulated for each scenario. Additionally, different SC deployment strategies were tested to evaluate their influence on system performance. The section concludes with a sensitivity analysis of the robust grid model, providing additional support to the results, and ends with a summary of the key findings presented in this chapter.

7.1 Scenario 1: Short-circuit Fault on Transmission Line Zone 31-32

This scenario involves a three-phase short-circuit with zero fault impedance, applied at the midpoint of the 400 kV transmission line connecting Zone 31 and Zone 32. The fault is initiated at 0.1 seconds and cleared at 0.15 seconds. Simulations were conducted under two system conditions: The base case and the N-1 contingency case, identified in the following pre-study. Furthermore, all three deployment strategies for SC were analysed: the centralized approach in Zone 32, the decentralized approach across Zones 31, 32, and 33, and a local connection at the bus to the wind power plant in Zone 32. The voltage response was evaluated at both the 400 kV bus in

Zone 32 and at the wind bus. This simulation was conducted to evaluate a severe voltage dip occurring in the nearby area of Zone 32.

7.1.1 Pre-study: N-1 Contingency Analysis

To better assess the contribution of external support, such as that provided by a SC, it is essential to analyse the system under various conditions. This includes both normal operation, referred to as the base case where all components function as expected, but also during more stressed scenarios. Analysing only the base case provides limited insight into the SC's potential, as the robust grid limits its impact due to its high system strength. Therefore, it becomes necessary to consider weakened operating conditions, where system strength is reduced. Such stressed conditions were created by disconnecting stable units or reducing available generation capacity, thereby making the system more vulnerable. To capture this, an N-1 contingency analysis was carried out, in which three potential component outages were simulated in Zone 32. The aim was to identify which of the disconnections would lead to the most critical operating condition. The following contingencies were considered:

- Disconnection of the pumped hydro plant
- Disconnection of the gas turbine
- Outage of the transmission line (TL) connecting Zone 32 and 33

The disconnection of elements did not lead to system instability, which is evident when observing Figure 7.1, where the pre-fault voltage remains close to 1 p.u. To further stress the system, the short-circuit fault in Scenario 1 was applied at 0.1 seconds. The resulting SCCs following the disconnection of various elements are presented in Table 7.1.

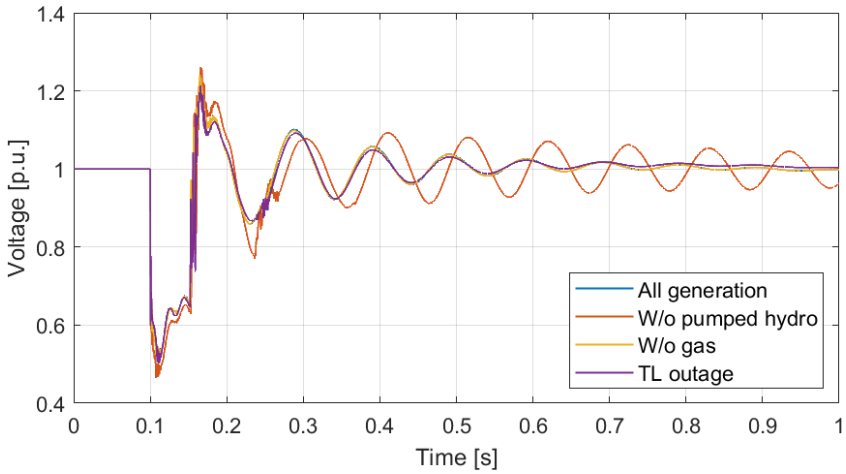

Figure 7.1: Voltage response to short-circuit fault for comparison of the different N-1 scenarios, measured at the 400 kV bus in Zone 32.

Table 7.1: SCC in Zone 32 following different N-1 contingency scenarios

Contingency	**SCC** [MVA]
W/o Pump. Hydro	7152
W/o Gas	9239
Outage TL	7056

The results indicate that the disconnection of the gas turbine and the outage of the transmission line have only a marginal impact on system performance in Zone 32. In contrast, the disconnection of the pumped hydro plant represents the worst-case scenario, as it introduces noticeable oscillations following fault clearance. This behaviour can likely be explained by the loss of a rotating machine, which directly impacts the system's inertia and affects the dynamics described by the swing equation. When the pumped hydro unit is disconnected, the SCC decreases from 9245 MVA to 7152 MVA. An interesting observation is that the outage of the transmission line causes the greatest decrease in SCC to 7056 MVA. However, while SCC serves as a useful measurement for system strength, it does not fully capture the dynamic behaviour. Based on this analysis, any subsequent reference to the disconnection of the pumped hydro plant will henceforth be referred to as the N-1 case.

7.1.2 67 MVA vs. 200 MVA

As two different sizes of SCs were evaluated in the grid model, an initial test was conducted to compare their performance under identical operating conditions. The results form a basis for comparing the two unit sizes and are essential for guiding the deployment strategy in later simulation scenarios. Figure 7.2a shows the voltage response at the 400 kV bus for the base case when compensating with three and six 67 MVA units, respectively. In contrast, Figure 7.2b illustrates the response when using one and two 200 MVA units. The choice of three and six 67 MVA units was made to enable a direct comparison with the total compensation capacity provided by one and two larger units, respectively. Additionally, due to the high SCC of the network, compensation using a single 67 MVA unit was considered insufficient. Its relative contribution to system strength was too small to make a measurable impact on voltage stability or fault response, thereby limiting its effectiveness in the intended analysis.

As observed in the results, the voltage responses of the two SC sizes are almost identical and difficult to distinguish. This similarity can primarily be explained by the fact that both units provide the same total amount of reactive power, resulting in comparable impacts on the voltage response. Another contributing factor may be that the larger unit is modelled by scaling up the parameters of the smaller SCs, which leads to similar dynamic behavior. Furthermore, as discussed during the SC verification, their control systems are tuned to produce comparable regulation responses to voltage variations. Consequently, it is not surprising that the responses of the two sizes are identical. Analysis of the results also indicates that scenarios involving a total compensation capacity below 200 MVA are not necessary to consider,

as such configurations would result in an even smaller impact on voltage stability than those already observed.

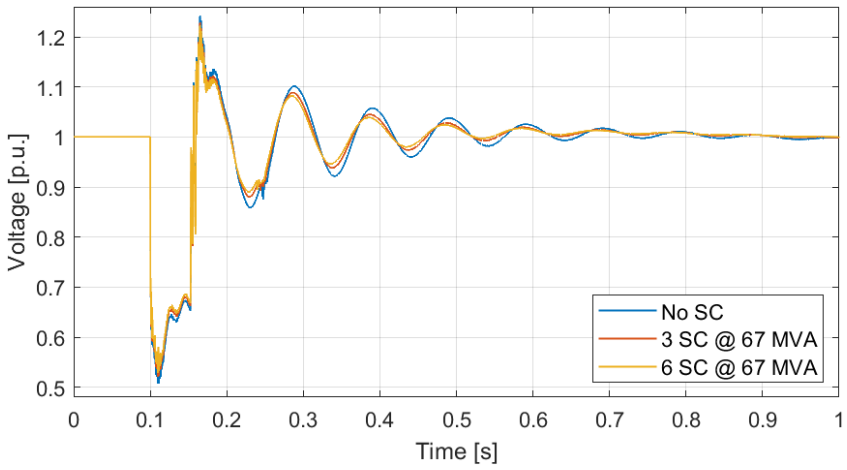

(a)

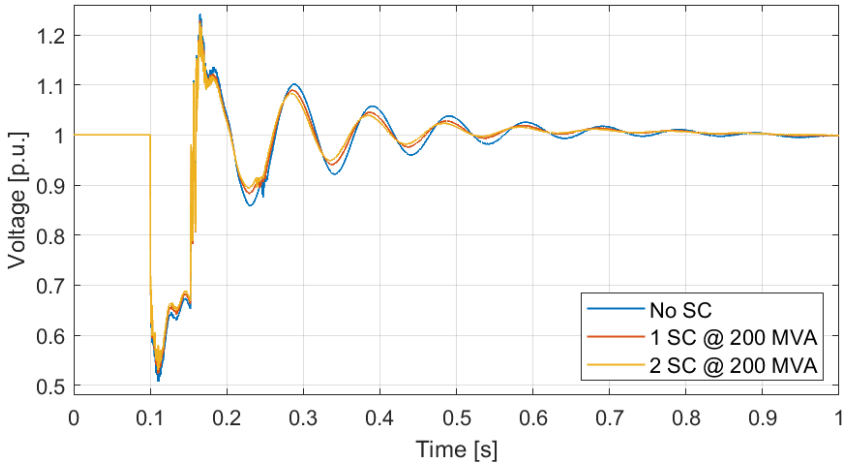

(b)

Figure 7.2: Voltage response to short-circuit fault, measured at the 400 kV bus in Zone 32, for base case with: **(a)** 67 MVA SCs and **(b)** 200 MVA SCs.

By observing the simulations alone, it is not possible to determine whether compensation with one larger unit or several smaller units is preferable. However, an important consideration is the increased redundancy provided by using multiple smaller units. Although the system under analysis is considered robust and the disconnection of one unit does not cause significant impact, in a more vulnerable grid, losing one large unit could lead to stability issues. In such cases, compensating with several smaller units is advantageous, as the disconnection of one unit still allows the remaining units to provide continued compensation.

7.1.3 Centralized vs. Decentralized

In addition to evaluating the performance of different SC unit sizes, a comparison is made to determine whether a decentralized approach using several smaller units distributed across multiple zones is more effective than a centralized solution with a single larger unit placed at a strategic location. Figure 7.3 illustrates the comparison between centralized and decentralized compensation strategies. In the centralized case two 200 MVA SCs with a total of 400 MVA are installed in Zone 32, while in the decentralized case the same total capacity is evenly distributed across Zones 31, 32 and 33 with two 67 MVA SCs installed in each zone.

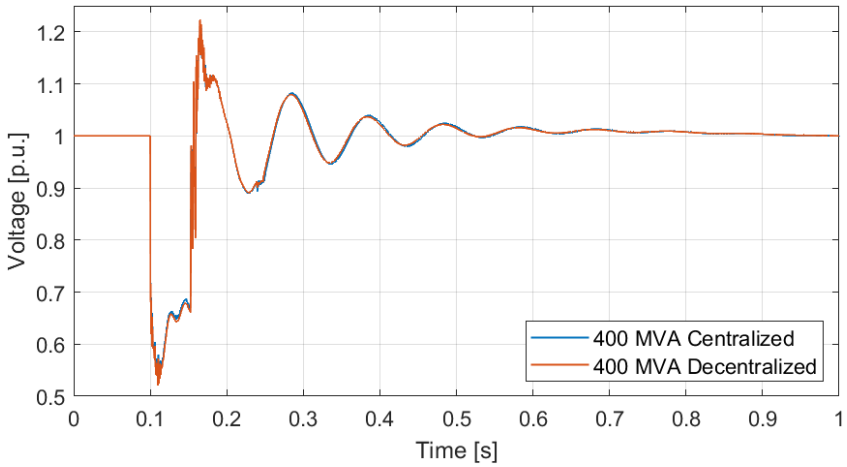

Figure 7.3: Comparison of a centralized and decentralized approach. Two 200 MVA SCs are placed in Zone 32 for the centralized, and two 67 MVA units are distributed each in zones 31, 32 and 33 for the decentralized approach. Voltage response measured at 400 kV bus in Zone 32.

As seen in Figure 7.3, there is no significant difference between the centralized and decentralized approaches, as the two voltage responses are nearly identical. Therefore, it is difficult to determine whether compensating with one larger unit or several smaller units is more beneficial based only on the simulation results. However, as mentioned earlier, deploying several smaller units provides important advantages in terms of system redundancy. This means that if one unit fails or is disconnected, the remaining units can continue to provide compensation, maintaining system stability and reducing the risk of voltage collapse. In contrast, disconnection of a single large unit can cause a significant impact, especially in already vulnerable systems, since the entire compensation capacity from that unit is lost at once. Thus, redundancy through multiple smaller units enhances the overall reliability and robustness of the power system, and are especially an important aspect in weaker grids such as the islanded grid model, presented in following chapter 8.

In addition, these results can be difficult to evaluate due to the limited impact of the SC in a robust power system, as also shown in Figure 7.2. Due to the relatively high SCC for the base case, the system is less sensitive to additional reactive power. As voltage varies locally and is affected by the reactive power balance at specific

nodes, its sensitivity varies throughout the network. In areas with high SCC and low voltage sensitivity, changes in reactive power have only a small effect on the local voltage profile. As a result, the differences between centralized and decentralized SC deployment approaches are difficult to observe under such conditions. For example, Figures 7.4a (base case) and 7.4b (N-1 case) demonstrate how placing an SC at the 33 kV wind bus leads to improved voltage support. At this weaker node, the SC's reactive power compensation has a greater influence on the voltage profile. The simulation time is increased for the N-1 case to ensure convergence.

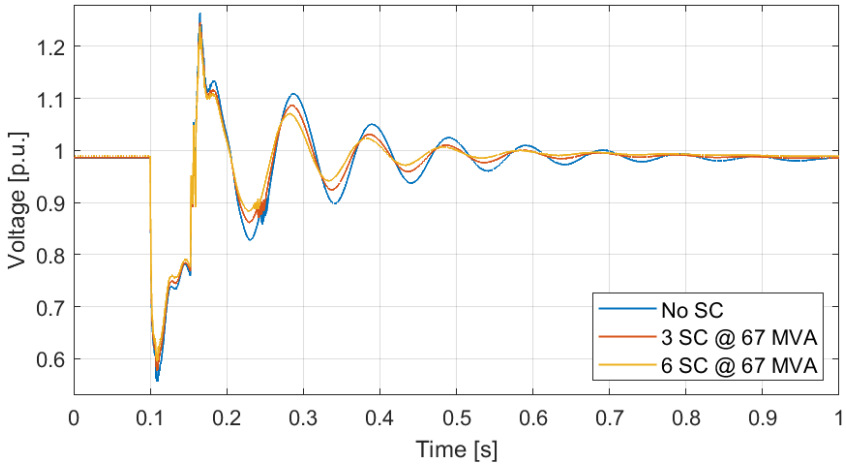

(a)

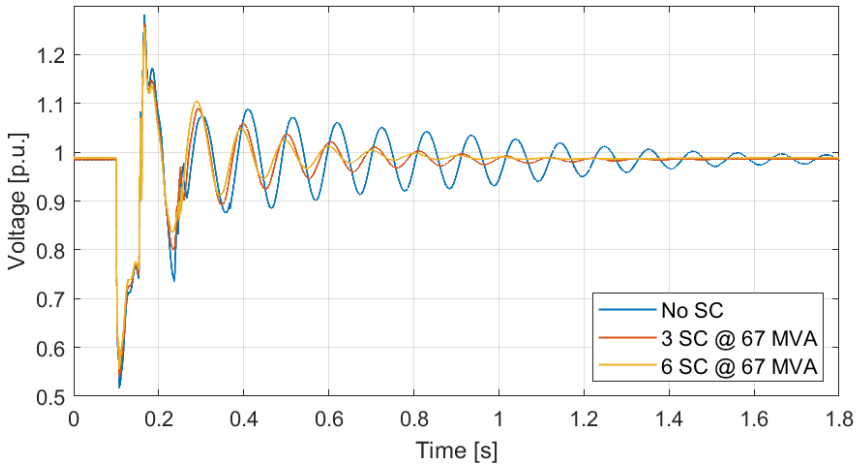

(b)

Figure 7.4: Voltage response to short-circuit fault, measured at the 33 kV wind bus, for: **(a)** Base case and **(b)** N-1 case.

As shown in Figure 7.4 above, the contribution from the SC becomes more pronounced in both the base case and the N-1 case when compensating at a weaker node. Due to its dynamic reactive power compensation, the voltage recovery after fault clearance is enhanced and easier to distinguish compared to compensation at the 400 kV bus. To improve voltage stability more effectively in a decentralized

approach, it is essential to place compensation units in more vulnerable parts of the grid where the need for reactive power is greater. This effect is further discussed in section 7.2. However, an interesting observation in this scenario, both seen when the SC is connected at the wind bus and the 400 kV bus, is the limited improvement during the actual fault. Since the fault occurs on a transmission line between Zone 32 and Zone 31, it is located close to the SC, with minimal impedance in between. This can cause the SC to inject a large current in an attempt to support the voltage dip. However, due to the low impedance, most of this current is instead fed directly into the fault, reducing its effectiveness in supporting voltage stability. In addition, evaluating faults located further from the compensation point, with greater impedance in between, provides a more realistic assessment of their impact on the voltage support of the actual fault.

7.2 Scenario 2: Short-circuit Fault on Transmission Line Zone 29-31

The second fault scenario involves a similar three-phase short-circuit fault with zero fault impedance, occurring on a transmission line located further away, between the adjacent Zone 31 and its neighbouring Zone 29. As in Scenario 1, the fault is initiated at 0.1 seconds and cleared at 0.15 seconds. This scenario is designed to evaluate the system's response to a less severe voltage dip resulting from a more distant fault, with greater impedance between the fault location and the observation point. Based on the conclusions from Scenario 1, only compensation using the 67 MVA SC unit is presented when connected to the wind bus in Zone 32. Additionally, the fault is simulated both for base case and the N-1 case. Figure 7.5a shows the voltage response observed at the 33 kV wind bus for the base case, with compensation from three or six 67 MVA units connected to the same bus as the wind power plant is connected to. In addition, Figure 7.5b shows the voltage response for the N-1 case.

As demonstrated in the results, the initial voltage dip caused by the fault for both the base case and N-1 case before connection of SC, is less severe in this scenario (0.65 p.u. and 0.64 p.u.) compared to scenario 1 (0.55 p.u. and 0.47 p.u). The implementation of SCs does not significantly mitigate the voltage dip, as also observed in Scenario 1. However, once the fault is cleared, the damping of voltage oscillations is improved, resulting in a shorter settling time before the voltage returns to normal operation within 0.95 - 1.05 p.u.

The limited impact of SCs on the actual fault can likely be explained by the overall robustness of the system, as previously discussed. This robustness is reflected in the relatively high SCC, even though Zone 32 and, in particular, the wind bus represent some of the weaker areas within the network. In both the base case and the N-1 scenario, the voltage dip remains almost unchanged when comparing no compensation to compensating with six units, from approximately 0.65 to 0.69 p.u for the base case, and 0.64 p.u. to 0.67 p.u for the N-1 case. While SCs contribute to I_{sc}, the high current demand during the fault possibly exceeds the SCs capacity

to significantly influence the actual fault. The SC's contribution to the I_{sc} is largely determined by its internal characteristics, such as subtransient reactance, X''_d, and also the transformer impedance, X_t. While the overall network strength affects the total system response, optimizing these parameters may increase its effectiveness in mitigating the voltage dip.

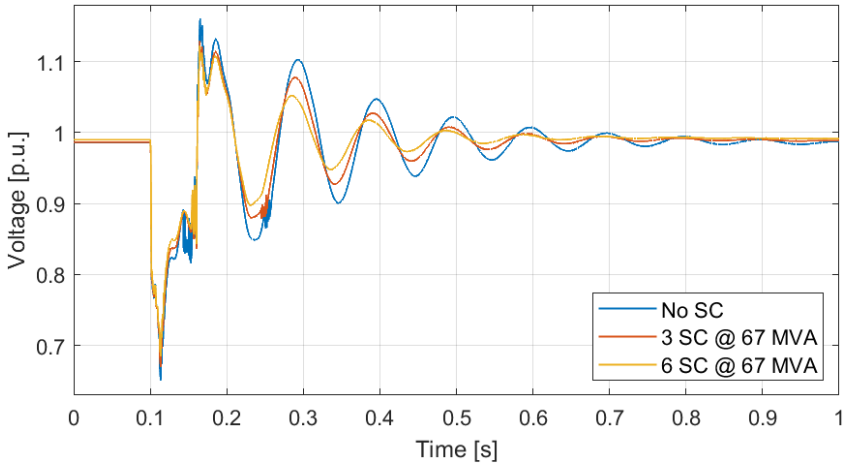

(a)

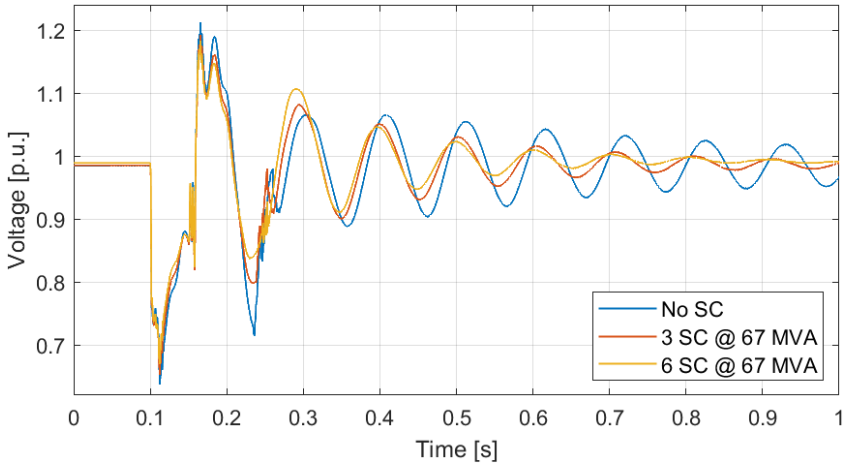

(b)

Figure 7.5: Voltage response to short-circuit, measured at the 33 kV wind bus, with compensation from 67 MVA SC for: **(a)** Base case and **(b)** N-1 case.

The reactive power support from the SC becomes more impactful after fault clearance, supporting voltage recovery and enhancing system damping. Therefore, the primary benefit of SCs in this context is not in mitigating the fault, but in improving post-fault voltage stability through dynamic reactive power support. The enhanced post-fault recovery observed, particularly in the N-1 case, can be explained by the SC's ability to rapidly inject or absorb reactive power via its excitation system, effectively regulating voltage deviations from the reference value. This reactive power

support increases the system's damping of oscillations, leading to faster stabilization and improved voltage recovery following the fault.

7.3 Scenario 3: Loss of Generation at Hydro Power Plant

The third and last fault scenario represents a generation loss at the hydro power plant located in Zone 32. This event occurs after 1 second, and represents a reduction of 0.85 p.u. in output torque of the synchronous generator, which directly corresponds to a generation drop of 0.85 p.u. As the primary objective of this fault is to analyse the system's frequency response, varying the location of the SC within Zone 32 had no significant impact on the results, as the frequency is a global parameter of the system, determined by the overall balance between generation and demand. Hence, only the deployment of the SC connected to the 400 kV bus is evaluated. In addition, due to the sustained system imbalance following the N-1 case, the frequency deviated permanently from 50 Hz to 49.9 Hz. Accurate frequency response analysis from the SC in the N-1 case was therefore not considered sufficient and hence only simulations for the base case are presented.

Figure 7.6 presents the frequency response following the generation loss. Inertia plays a crucial role in the power system's initial response to frequency deviations. Since the SC contributes to frequency regulation only through its inertial response, the first few seconds following a disturbance are especially important for analysis. The frequency does not fully return to 50 Hz after the disturbance but instead stabilizes around 49.95 Hz after the initial seconds visible in the figure. This behaviour suggests a lack of generation or insufficient secondary frequency control to restore the system to its nominal frequency. However, important to take into consideration that the frequency remains within acceptable operating limits as it is operates within 49.5 and 50.5 Hz.

Illustrated in Figure 7.6, is that an increase in total system inertia H_{sys} leads to an improvement in the RoCoF, consistent with the swing equation and equation (2.4). Consequently, this results in an improved f_{nadir}. A higher f_{nadir} allows the system more time to respond to frequency deviations, which reduces the risk of reaching critical frequency thresholds. According to equation (2.7), the total system inertia is determined by all machines in the grid that contribute with inertia. In a strong grid that already includes a large number of synchronous generators, influencing the overall system inertia is inherently more challenging compared to a smaller or islanded grid, despite 67 MVA and 200 MVA SCs having inertia constants of 7.046 and 8.024 seconds, which are higher than those of the generators in the system. The installation of six SCs rated at 67 MVA results in a 2.04% increase in H_{sys}, which corresponds to an improvement in RoCoF by 0.05 Hz/s. Therefore, achieving more significant improvements in RoCoF and f_{nadir} would require a much greater contribution to system inertia. In a strong grid, this would involve the installation of a large number of additional SC.

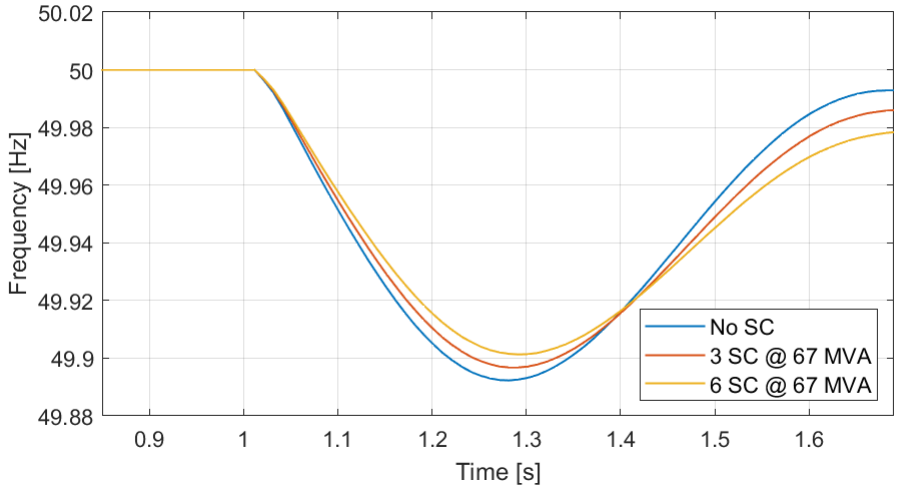

Figure 7.6: Frequency response to generation loss from hydro power plant with 0.85 pu, compensation with 67 MVA SC.

Values for RoCoF, f_{nadir} and H_{sys} are presented in Table 7.2. This was also analysed for the 200 MVA SC, however the results showed similar behaviour and are therefore not presented. As shown in the table, the inertial contribution from the SC, which accounts for approximately 1-2% of the total system inertia, indicates that its overall impact during such events is limited.

Table 7.2: Results following a generation loss regarding RoCoF, f_{nadir} and H_{sys} when connecting SCs.

SCs	**RoCoF** [Hz/s]	$\boldsymbol{f_{nadir}}$ [Hz/s]	$\boldsymbol{H_{sys}}$ [s]	**% of** $\boldsymbol{H_{sys}}$ [%]
0	0.37	49.89	12.50	-
3	0.34	49.90	12.63	1.03
6	0.32	49.91	12.76	2.04

Additionally, it is essential to analyse the system's voltage response during such an event to ensure that it does not lead to system instability. Figure 7.7 illustrates the voltage response with and without SCs implemented, following a 0.85 p.u. loss at the hydro power plant. Although there is a loss of generation in Zone 32, the voltage response remains stable within the range of 0.95 - 1.05 p.u. This is primarily due to that voltage is more sensitive to changes in reactive power, and this fault represents a loss of active power. As seen in earlier scenarios for the base case, small deviations in voltage, around 1 p.u, can be efficiently damped by the system strength and units supporting reactive power. Hence, a change in voltage from 1 to 1.01 p.u. is not considered problematic and therefore not further analysed.

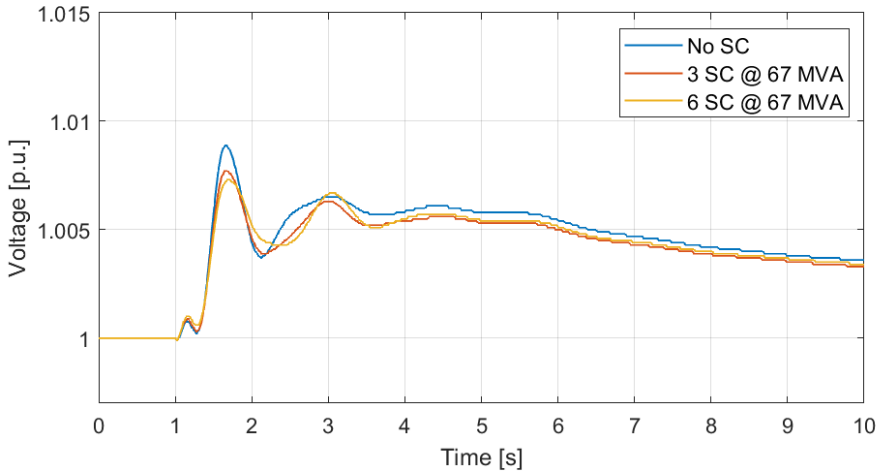

Figure 7.7: Voltage response to generation loss from hydro power plant with 0.85 pu, measured at the 400 kV bus in Zone 32 when compensation with 67 MVA SC.

7.4 Sensitivity Analysis

A sensitivity analysis was carried out to assess how the voltage at a specific node in the system responds to reactive power injection. This was performed by conducting a QV-analysis in PowerFactory for the various deployment locations considered in the study, serving as a validation reference for the simulation results. To visually illustrate the relationship between voltage and reactive power in the system, Figure 7.8 presents the QV-curve for the bus in Zone 32. As observed, the implementation of SCs increases the stability margin to voltage collapse. Table 7.3 presents the values of dV/dQ and the operating voltage for each deployment location in the robust grid model.

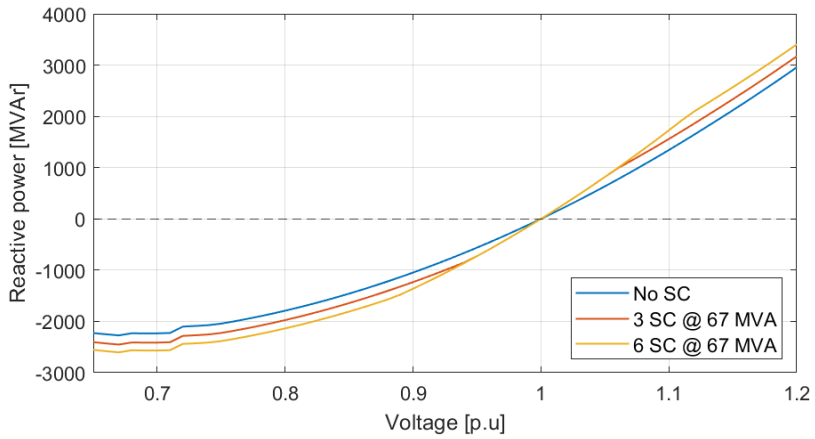

Figure 7.8: QV-curve for different numbers of SCs with 67 MVA rating, showing the reactive power as a function of voltage at main bus in zone 32. The dashed line represents the reference for zero reactive power.

Table 7.3: Voltage sensitivity dV/dQ and SCC at the buses in the robust grid model without SCs.The dV/dQ values are evaluated near 1.00 p.u. and represent the local sensitivity of voltage to reactive power injections.

Location	**Voltage** [kV]	**dV/dQ** [p.u./MVAr]
32, Main Bus	400	0.000086
32, Wind Bus	33	0.000124
31, Main Bus	400	0.000031
33, Main Bus	400	0.000044

The calculations are based on a system condition with reactive power close to 0 MVAr, corresponding to a voltage of approximately 1 p.u. This reflects typical operating conditions, making the resulting voltage sensitivity to reactive power injection at the SC location a relevant and representative measure. Low dV/dQ values close to zero indicate that a large amount of reactive power is required to produce notable changes in the voltage. These results confirm what has been observed in the simulations, highlighting the robustness of the system and the limitations of the SC in such a network. Important to take into consideration is that these voltage sensitivity values are calculated for the linear region, close to where voltage is 1 p.u. During a fault, the voltage is lower and no longer in the linear region as it is closer to the stability limits of the QV-curve. Consequently, the dV/dQ values are more relevant for the post-fault recovery when the voltage oscillates around its nominal value.

7.5 Summary

The simulations in the robust grid model prove that SCs can contribute with voltage and frequency support, thanks to its ability to dynamically support reactive power as well as support the overall inertia of the system. The simulations highlight the importance of strategic deployment strategies, especially in a strong network, as the contribution from the SC otherwise is limited by the overall system strength.

No significant performance difference was observed between the 67 MVA and 200 MVA SCs when providing equal reactive power. However, using multiple smaller units improves redundancy, as the loss of a single large unit can impact stability. While the system is strong enough to withstand such events, this becomes crucial in weaker grids, where the loss of a single large SC can have more severe impacts on voltage stability and dynamic performance.

The SC's impact during short-circuit events was mainly seen after fault clearance, improving post-fault voltage recovery. Its effect on the initial voltage dip caused by the fault was limited due to the system's high SCC, even under weakened conditions. Possibly, this was also limited by low impedance between the fault and the SC, due

to the short distance. However, its dynamic reactive power support effectively improved post-fault oscillations and reduced recovery time. Placement proved critical, and installation at the 33 kV wind power plant bus notably improved performance, especially in the N-1 case, while the 400 kV bus offered limited benefit. These results highlight the importance of deploying SCs in more vulnerable areas with lower voltage levels and reduced SCC to enhance voltage stability in a robust power system. The sensitivity analysis and the dV/dQ values confirm the observations from the results, demonstrating that reactive power has a greater impact on voltage at weaker points in the system. However, in general, it is expected to achieve small changes in voltage in such a robust grid.

When observing a loss of generation, the SC supports the frequency through its inertial response. However, since the grid already has high H_{sys}, from the existing synchronous generators, the SC's contribution, around 1-2% of the total inertia, has limited effect. To make a larger impact on frequency stability, many more SCs would be needed. Additionally, when analysing the voltage response, the system remains stable within 0.95 to 1.05 p.u. even after the generation loss because the fault mainly affects active power, while voltage is more sensitive to reactive power changes. These small changes around 1 p.u. are not considered critical.

8

Simulations Results from Islanded Grid Model

Following the results and analysis of the robust grid model in Chapter 7, this chapter presents the RMS simulation results conducted in PowerFactory for the islanded grid model. As outlined in earlier chapters, three scenarios have been investigated to evaluate both frequency and voltage behaviour before and after the connection of the 8 MVA SC. The tested fault scenarios are as follows:

- **Scenario 1:** A three-phase short-circuit fault on the underground cable LO-OI 1, which connects Bus 2 and Bus 4.
- **Scenario 2:** A hydropower plant trip resulting in a generation loss corresponding to a mechanical torque of -0.8 p.u.
- **Scenario 3:** A decrease of one load, located at Bus 2, corresponding to 3.8% loss of total system load.

The chapter concludes with a voltage sensitivity analysis, presenting QV-curves and the corresponding dV/dQ values, to further evaluate the impact of the SC on voltage stability in the grid. Finally, a brief chapter summary is provided to highlight the key findings from the simulations in the islanded grid model.

8.1 Scenario 1: Short-circuit Fault on Cable LO-OI 1

The first scenario involves a three-phase short-circuit fault of one of the parallel underground cables connecting the oil area and load area (Bus 2 and Bus 4), named LO-OI 1. The fault occurs at 1 second and lasts for 150 ms before the fault is cleared. The first analysis evaluates the effect of disconnecting each of the three generation types in the system, one at a time. Figure 8.1a shows the case without any SCs connected. In each simulation, one generating source was disconnected, leaving only the remaining two in operation. The voltage response is measured at Bus 1, located in the central area. Figure 8.1b presents the same set of cases, but with an 8 MVA SC connected to Bus 1. This test was conducted to evaluate how the impact of the SC varies depending on the system's generation characteristics.

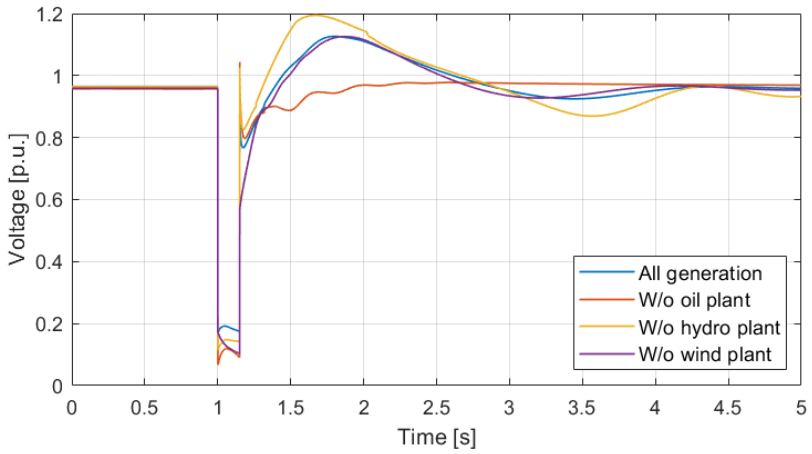

(a)

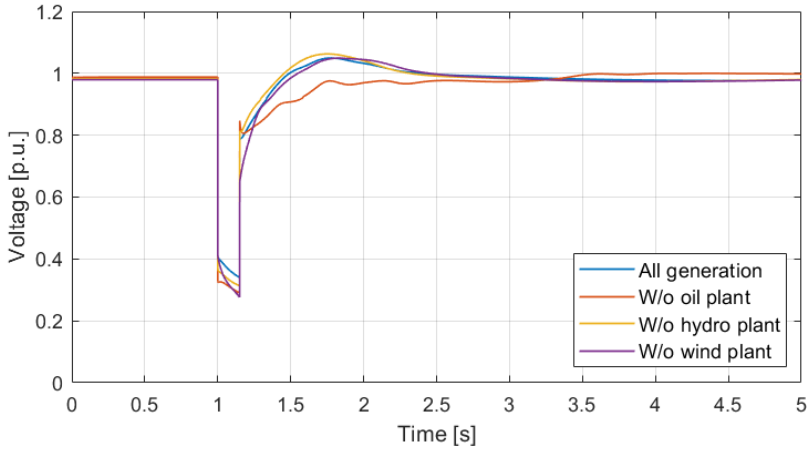

(b)

Figure 8.1: Voltage response at Bus 1 of a short-circuit fault following disconnection of generation for: **(a)** without SC and **(b)** with 8 MVA SC located at Bus 1 in the central area.

By analysing the figures, it is clear that the SC significantly improves voltage stability by mitigating both the initial voltage dip and the post-fault oscillations. Immediately after the fault, the voltage drop is less severe with the SC in operation, reaching only about 0.3 p.u., compared to 0.1 p.u. without it. The voltage peak that follows the fault is also noticeably reduced, particularly in scenarios where the hydro plants are disconnected. In that case, the peak is lowered from 1.2 p.u. to 1.07 p.u. When the oil plant is disconnected, a 100% RES system is simulated, with only hydro and wind as generation sources. In this case, the voltage does not show an overshoot following fault clearance. Additionally, the system stabilizes more quickly. The settling time after fault clearance is shortened from approximately 3.35 seconds to 1.35 seconds for all cases when the SC is connected.

A possible explanation for why the system is most affected by the disconnection of the hydropower plants is that, in the islanded grid model, the oil power plant's

AVR gain is significantly higher than that of the other generators in the system. This highly responsive AVR response may contribute to the increased oscillatory behaviour observed when the hydro units are removed. Conversely, in the scenario where the oil plant is disconnected, the remaining hydro units are equipped with relatively low AVR gains, resulting in a slower but more stable voltage response with minimal oscillations. Furthermore, the wind power plants do not contribute to the reactive power, and both the hydro and oil power plants provide limited reactive power support, which reduces the system's ability to maintain voltage stability during the disturbance. During the short-circuit fault, the SC contributes with instantaneous I_{sc}, helping to mitigate the voltage dip. However, due to the delay in the excitation system, typically a few hundred milliseconds, the SC does not provide dynamic reactive power support during the fault itself. Instead, the excitation system begins responding once the fault is cleared, enabling the SC to contribute to post-fault voltage recovery. This reduces the oscillations and shortens the settling time, as seen in the figures. These results highlight the SC's ability to enhance system stability under severe disturbances, such as short-circuit faults. This improvement is observed consistently across all three generation mix scenarios, including the case without the oil plant, which represents a 100% renewable energy system.

For the same fault scenario, an additional case was simulated to compare the voltage behaviour at Bus 1 in the central area when up to three SCs were connected in a decentralized way, compared to only one SC in the previous case. In this case, all generators are connected and operating. The first SC was connected to Bus 1, the second to Bus 3, and the third to Bus 2, increasing the number of SCs for each simulation shown in Figure 8.2.

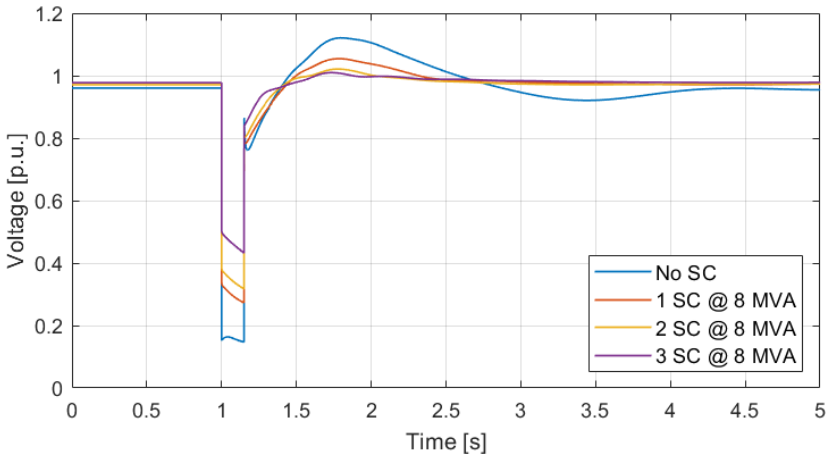

Figure 8.2: Voltage at Bus 1 in the central area during a short-circuit fault, comparing the effect of adding one, two, and three SCs in a decentralized configuration.

The case without any SC shows the lowest voltage drop following the fault, with a minimum voltage of 0.15 p.u. and the value increases for each SC added. The results

indicate that adding more SCs mitigates the voltage drop further and accelerates the voltage recovery. The most significant improvements post-fault are observed when adding one or two SCs. Adding a third unit provides limited additional post-fault improvement for the analysed bus, although it does further reduce the initial voltage dip by contributing to I_{sc}. Worth noticing is that when connecting the SC to Bus 3 in the hydro area (yellow curve), it shows less improvement for the voltage dip compared to the other cases. This is likely because Bus 3 is located furthest away from the observed bus, and hence there is more impedance between the observation point and the SC, limiting its I_{sc} contribution. Another explanation for this could be that the hydro area only has a 10.5 kV bus, meaning that the SC is connected to a lower voltage compared to the other SCs and the observed 21 kV bus.

A case where the SCs were placed in a centralized configuration, connected to the same bus, was also tested for all three cases but showed no significant improvement in the voltage response compared to the result in Figure 8.2 above. Since the buses in the islanded grid model are connected via short cables ($<$ 18 km), the electrical distance between them is relatively small. As a result, reactive power support provided at one location has a more system-wide influence, rather than being concentrated to only the local bus. Distributing the SCs across multiple buses not only improves local voltage support and dynamic response but also enhances system redundancy as discussed in Chapter 7. In the event of a fault or outage at one location, decentralized placement ensures that other SCs can continue to support the grid, increasing overall reliability.

8.2 Scenario 2: Loss of Generation HYDRO G1

Figure 8.3 shows the system frequency response following the trip of the hydropower plant HYDRO G1, corresponding to a generation loss of 0.8 p.u. torque. This loss, occurring at 2 seconds, remains constant throughout the simulation. Because of this loss, other generators in the system have to increase their output power to compensate, leading to a more strained system. Four cases are compared: without an SC, and with one, two, and three SC units connected to Bus 1, Bus 4 and Bus 2, respectively. In the absence of additional inertia, as in the first case seen in the figure, the frequency drops rapidly, reaching a f_{nadir} of 48.71 Hz and a RoCoF of 1.554 Hz/s, both of which fall outside the acceptable range defined by the grid code. As the number of SCs increases, both RoCoF and f_{nadir} improve significantly. With three units connected, the RoCoF is reduced to 0.274 Hz/s and f_{nadir} increases to 49.43 Hz. Regarding RoCoF improvement, only one SC would be sufficient to improve the value to a value within the 1 Hz/s limit. Regarding f_{nadir}, more SCs would be required to come closer to 49.5 Hz in this scenario. These improvements can be explained by the additional rotational inertia and thus the higher value of H_{sys}. A summary of all RoCoF and f_{nadir} values is presented in Table 8.1.

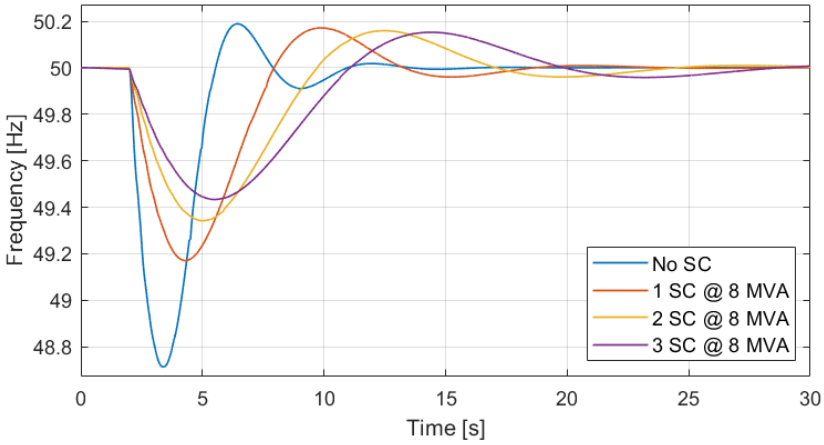

Figure 8.3: Frequency response following a -0.8 p.u. hydro generation loss with varying numbers of connected SCs.

As also seen in Figure 8.3 above, it is important to note that damping worsens slightly as more SC units are connected. This leads to frequency overshoots and longer settling times. An explanation to this could be that multiple SCs may interact unfavourably with existing AVR or other control systems if not properly tuned. Poor coordination or tuning of these controllers can introduce oscillatory behaviour or further reduce damping in the system. Another possible explanation for the observed behaviour is the lack of power system stabilizers (PSS) in the generator and SC control systems in the islanded grid mode.

However, while SCs do not contribute to primary or secondary frequency control due to the lack of active power output, their inertial response significantly shapes the frequency trajectory following a disturbance. According to the swing equation and equation (2.4), the RoCoF is inversely proportional to total system inertia H_{sys}. Thus, by increasing H_{sys}, SCs reduce the RoCoF and extend the time to reach f_{nadir}. This delay allows more time for governor-controlled generators to respond, resulting in a smoother frequency behaviour and improved overall frequency stability, even beyond the inertial response phase. Since this small islanded model has few dynamic generators, the frequency controls are limited. Table 8.1 also lists the increase of H_{sys} when SC are incrementally added to the system.

Table 8.1: Results following a generation loss regarding RoCoF, f_{nadir} and H_{sys} when connecting SCs.

SCs	**RoCoF** [Hz/s]	$\boldsymbol{f_{nadir}}$ [Hz/s]	$\boldsymbol{H_{sys}}$ [s]
0	1.554	48.71	3.128
1	0.594	49.17	4.360
2	0.368	49.34	4.807
3	0.274	49.43	5.039

Figure 8.4 shows the voltage response following the same scenario as described for the frequency case above. As previously noted, a loss of generation primarily impacts frequency stability, which becomes evident in the figure. However, without any SCs the voltage settles at a relatively low steady-state level. This behaviour can be explained by the low reactive power support in the original islanded grid model due to the disconnection of the original SC, as discussed in Chapter 6. As more SCs are connected, the steady-state voltage increases progressively towards 1 p.u. The SC also limits the voltage oscillations caused by the fault. The generation loss causes only minor voltage oscillations shortly after the fault, but the system stabilizes quickly in all cases. This further demonstrates that while generation loss affects voltage stability to a lesser extent, the inclusion of SCs contributes positively to maintaining acceptable voltage levels and limits voltage oscillations.

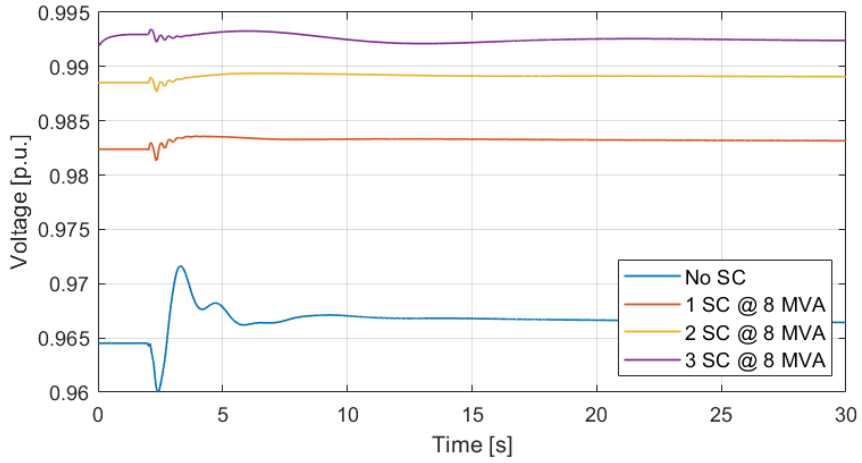

Figure 8.4: Voltage response at Bus 1 following a 0.8 p.u. hydro generation loss with varying numbers of connected SCs.

8.3 Scenario 3: Loss of Load

In this final scenario, a sudden load reduction occurs in the oil area at 2 seconds, resulting in a temporary energy overproduction and a corresponding frequency increase, as shown in Figure 8.5. The 30% load reduction at Bus 2 corresponds to a decrease of 150 kW and 72.6 kVAr, which is equivalent to approximately 3.8% of the total system active and reactive load. This relatively small, localized disturbance is used to assess frequency stability under a typical load rejection event.

The frequency response is shown in Figure 8.5. Immediately after the disconnection, the frequency rises to a maximum of 50.23 Hz and then settles at a f_{nadir} of 49.96 Hz in the case without any SCs. Both values remain within the acceptable limits for normal operation as defined by the grid code. A summary of RoCoF and f_{nadir} values is presented in Table 8.2. The corresponding H_{sys} values are also included for consistency, although they are identical to those listed for Scenario 2. To evaluate the impact of SC integration, the first SC was connected to Bus 2 in the oil area

and the second to Bus 4 in the load area. These areas are connected via an 18 km cable. As seen in the figure, the implementation of an SC significantly reduces the frequency overshoot following the load rejection. Although none of the simulated cases violate grid code frequency requirements, the addition of SCs leads to a clear improvement in overall frequency behaviour. However, similarly to the generation loss in Scenario 2, the addition of the SC introduces damping issues, as seen in the figure. This suggests that, as before, the islanded grid model either lacks power system stabilizers or that their tuning and coordination could be improved.

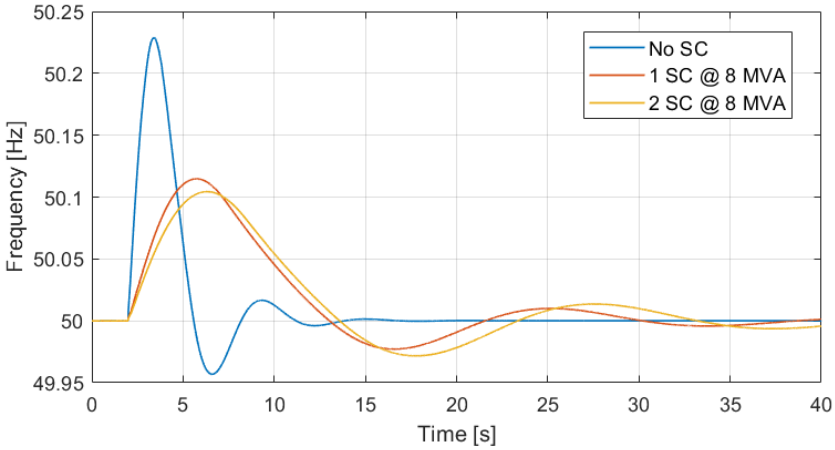

Figure 8.5: Frequency response following a 30% load decrease of a load in the oil area, with varying numbers of SCs implemented.

Lastly, the marginal benefit of adding more than one SC is limited, with minimal additional improvement observed beyond the first unit. The small frequency deviations in all cases are primarily due to the relatively small size of the disturbance. Larger load rejection events were considered during the study, but introduced convergence issues and simulation errors. Therefore, this scenario was selected as the most suitable for stable analysis.

Table 8.2: Results following a loss of load regarding RoCoF, f_{nadir} and total system inertia when connecting SCs.

SCs	**RoCoF** [Hz/s]	$\boldsymbol{f_{nadir}}$ [Hz/s]	$\boldsymbol{H_{sys}}$ [s]
0	0.258	49.96	3.128
1	0.047	49.97	4.360
2	0.037	49.98	4.807

8.4 Sensitivity Analysis

To further study the impact of SCs have on voltage stability in the islanded grid model, a QV-curve showing the implementation of one or two SCs at Bus 1 compared to the case with no SCs connected. From Figure 8.6 it is evident that with the

installation of more SCs in the system, the safety margin to the voltage stability limit increases, meaning that the system can tolerate larger reactive power disturbances without risking voltage collapse, indicating a stronger grid. Bus 1 in the central area is studied for all three cases in the figure.

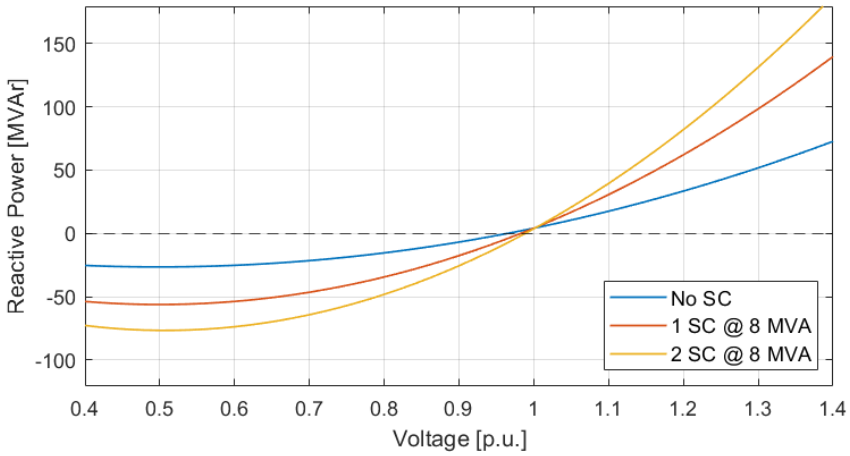

Figure 8.6: QV-curve for increasing numbers of SCs with 8 MVA rating, showing the reactive power as a function of voltage. The dashed line represents the reference for zero reactive power.

As a supplement to the dynamic simulations, a steady-state sensitivity analysis based on dV/dQ is also performed to validate the results. Table 8.3 summarizes the dV/dQ values at key buses in the system before any SCs are installed. Compared to the dV/dQ values in the robust grid model, the islanded grid shows approximately 100 times higher voltage sensitivity to reactive power injection (0.000086 vs. 0.00873 vs p.u./MVAr) when comparing Zone 32 in the robust grid and Bus 1 in the islanded grid. This indicates that SCs have a significantly greater influence on voltage in weaker grid conditions, further supporting the findings presented in this chapter.

Table 8.3: Voltage sensitivity dV/dQ and SCC at the buses in the islanded grid model without SCs.The dV/dQ values are evaluated near 1.00 p.u. and represent the local sensitivity of voltage to reactive power injections.

Bus	**Voltage** [kV]	**dV/dQ** [p.u./MVAr]
1	21	0.00837
2	21	0.00742
3	10.5	0.02896
4	21	0.00866

8.5 Summary

The simulation results confirm that SCs significantly enhance both frequency and voltage stability in the islanded grid model. Connecting SCs significantly improves voltage stability during short-circuit faults and the disconnection of generation units in the islanded grid. With one 8 MVA SC connected to the central area, the voltage dip is reduced, post-fault overshoot is lower, and settling time is reduced. Adding SCs in a decentralized configuration further improves voltage support. Since the SC injects and absorbs reactive power at the point of connection, installing several 8 MVA units at the same bus in the islanded grid model is not sufficient, as it showed no significant improvement compared to the decentralized case. From a system stability perspective, it is more effective to distribute the SCs in a decentralized way across different locations in the network, rather than concentrating them at a single bus.

In the generation loss case, SCs had a substantial impact on improving frequency response. RoCoF was significantly reduced and the f_{nadir} improved with each added SC. However, increasing the number of SCs also introduced more oscillations and reduced damping. This effect is likely due to the absence of coordinated control mechanisms, such as power system stabilizers or correctly tuned control systems. Although the generation loss had a limited impact on voltage response, the SCs improved steady-state voltage levels by injecting reactive power.

For the loss of load scenario, the disturbance corresponds to only 3.8% of the total system load, simulating a small disturbance. Introducing one SC at Bus 2 notably improved the frequency response by reducing the overshoot. However, adding more than one SC yields minimal additional benefit. Similar to the generation loss case, the SC introduces damping issues, suggesting that the islanded grid lacks a properly tuned control system and power system stabilizers.

9
Conclusions

This thesis evaluated the ability of synchronous condensers (SCs) to improve voltage and frequency stability in two contrasting power system configurations. The first represents a large, strongly interconnected grid, while the second is a smaller islanded system with limited SCC and inertia. For each grid model, fault scenarios were applied to assess the system response before and after the connection of SCs.

The potential for stability enhancement from SCs depends primarily on their capacity relative to system conditions. The robust grid model is inherently too strong to benefit significantly, even with multiple units connected. Both the 67 MVA and 200 MVA SCs show a relatively small impact in a system with an SCC of approximately 10000 MVA. Similarly, the SCs contribution to H_{sys} remains small in the robust grid model, limiting their effect on RoCoF and f_{nadir} even though they separately have large inertia constants. Consequently, SCs primarily offer supplementary support rather than substantial improvement. In contrast, the 8 MVA SC in the islanded grid model is connected to a much weaker system with an SCC of around 45 MVA, making its contribution proportionally far more significant. The SC leads to increased H_{sys}, which improves both RoCoF and f_{nadir}, providing essential frequency support.

The simulation results for the robust grid model indicate that the most significant improvements in voltage stability occur during post-fault recovery, where SCs enhance voltage restoration. This effect was most pronounced when SCs were connected to weaker points in the system, such as the point of connection at the wind power plant, characterized by lower voltage levels and short-circuit capacity. Further improvements were also observed under weakened operating conditions. The comparison between 67 MVA and 200 MVA compensation units showed similar responses, making it difficult to distinguish their performance. However, deploying multiple smaller units offers advantages in terms of redundancy, as the disconnection of a single unit has a smaller impact on overall system stability.

The study also concludes that placing one 8 MVA SC in the central area of the islanded grid model significantly improved the voltage response during and after the short-circuit fault in all cases and for all generation mixes, even in the scenario where the oil plant was disconnected, simulating a 100% RES system. Adding more 8 MVA units in a decentralized way further reduced the initial voltage dip and improved settling time. Due to the small system size and short electrical distances between buses, similar results were also observed when multiple SCs were placed at a single bus.

9.1 Future Work

While this thesis provides insights into the performance of SCs in two contrasting power systems, several areas remain open for future work. One promising direction would be to investigate the effects of decentralized SC placement in distribution networks with lower voltage levels. Additionally, applying the analysis to a larger grid model with a higher share of RES could offer deeper insight into how SCs can contribute to system stability under higher RES penetration due to fewer synchronous generators contributing to system inertia and short-circuit current. Lastly, a study examining the combination of SCs with BESS in a hybrid solution could be valuable, enabling both reactive and active power support to enhance overall dynamic performance.

References

[1] IEA, *Renewables 2024*, Licence: CC BY 4.0, 2024. [Online]. Available: https://www.iea.org/reports/renewables-2024.

[2] L. Mehigan, J. Deane, B. Gallachóir, and V. Bertsch, "A review of the role of distributed generation (dg) in future electricity systems," *Energy*, vol. 163, pp. 822–836, 2018, ISSN: 0360-5442. DOI: https://doi.org/10.1016/j.energy.2018.08.022.

[3] ABB. "Deploying synchronous condensers to provide distributed power grid support." Accessed: 2024-05-12. (2020), [Online]. Available: https://search.abb.com/library/Download.aspx?DocumentID=9AKK108141.

[4] K. S. Ratnam, K. Palanisamy, and G. Yang, "Future low-inertia power systems: Requirements, issues, and solutions - a review," *Renewable and Sustainable Energy Reviews*, vol. 124, p. 109 773, 2020, ISSN: 1364-0321. DOI: https://doi.org/10.1016/j.rser.2020.109773.

[5] N.-A. Masood, S. U. Mahmud, M. N. Ansary, and S. R. Deeba, "Improvement of system strength under high wind penetration: A techno-economic assessment using synchronous condenser and svc," *Energy*, vol. 246, p. 123 426, 2022, ISSN: 0360-5442. DOI: https://doi.org/10.1016/j.energy.2022.123426. [Online]. Available: https://www.sciencedirect.com/science/article/pii/S0360544222003292.

[6] ABB, *Abb synchronous condensers*, Accessed: 2025-01-28, 2024. [Online]. Available: https://new.abb.com/motors-generators/synchronous-condensers.

[7] H. Soleimani, D. Habibi, M. Ghahramani, and A. Aziz, "Strengthening power systems for net zero: A review of the role of synchronous condensers and emerging challenges," *Energies*, vol. 17, no. 13, 2024, ISSN: 1996-1073. DOI: 10.3390/en17133291.

[8] P. S. Kundur and O. P. Malik, *Power System Stability and Control*. McGraw Hill, 2022.

[9] S. Teleke, T. Abdulahovic, T. Thiringer, and J. Svensson, "Dynamic performance comparison of synchronous condenser and svc," *IEEE Transactions on Power Delivery*, vol. 23, no. 3, pp. 1606–1612, 2008. DOI: 10.1109/TPWRD.2007.916109.

[10] M. Nedd, C. Booth, and K. Bell, "Potential solutions to the challenges of low inertia power systems with a case study concerning synchronous condensers," in *2017 52nd International Universities Power Engineering Conference (UPEC)*, 2017, pp. 1–6. DOI: 10.1109/UPEC.2017.8232001.

[11] DIgSILENT GmbH. "Powerfactory." Accessed: 2025-05-06. (2025), [Online]. Available: https://www.digsilent.de/en/powerfactory.html.

[12] P. Kundur, J. Paserba, V. Ajjarapu, *et al.*, "Definition and classification of power system stability ieee/cigre joint task force on stability terms and definitions," *IEEE Transactions on Power Systems*, vol. 19, no. 3, pp. 1387–1401, 2004. DOI: 10.1109/TPWRS.2004.825981.

[13] N. M. Tabatabaei, A. J. Aghbolaghi, N. Bizon, and F. Blaabjerg, Eds., *Reactive Power Control in AC Power Systems: Fundamentals and Current Issues* (Power Systems). Springer International Publishing, 2017. DOI: 10.1007/978-3-319-51118-4.

[14] G. Poyrazoglu and H. Oh, "Optimal topology control with physical power flow constraints and n-1 contingency criterion," *IEEE Transactions on Power Systems*, vol. 30, no. 6, pp. 3063–3071, 2015. DOI: 10.1109/TPWRS.2014.2379112.

[15] National Energy System Operator (NESO), *The Grid Code*, Issue 6, Revision 31, 2025. [Online]. Available: https://dcm.nationalenergyso.com/.

[16] V. Knap, S. K. Chaudhary, D.-I. Stroe, M. Swierczynski, B.-I. Craciun, and R. Teodorescu, "Sizing of an energy storage system for grid inertial response and primary frequency reserve," *IEEE Transactions on Power Systems*, vol. 31, no. 5, pp. 3447–3456, 2016. DOI: 10.1109/TPWRS.2015.2503565.

[17] L. Mehigan, D. Al Kez, S. Collins, A. Foley, B. Ó'Gallachóir, and P. Deane, "Renewables in the european power system and the impact on system rotational inertia," *Energy*, vol. 203, p. 117 776, 2020, ISSN: 0360-5442. DOI: https://doi.org/10.1016/j.energy.2020.117776.

[18] A. Ulbig, T. S. Borsche, and G. Andersson, "Impact of low rotational inertia on power system stability and operation," *IFAC Proceedings Volumes*, vol. 47, no. 3, pp. 7290–7297, 2014, ISSN: 1474-6670. DOI: https://doi.org/10.3182/20140824-6-ZA-1003.02615.

[19] ENTSO-E, "Inertia and Rate of Change of Frequency (RoCoF)," European Network of Transmission System Operators for Electricity (ENTSO-E), Tech. Rep., version 17, Dec. 2020, Accessed: 2025-02-18. [Online]. Available: https://eepublicdownloads.entsoe.eu/clean-documents/SOC%20documents/Inertia%20and%20RoCoF_v17_clean.pdf.

[20] S. Yang, Q. Meng, Y. Zhang, Z. Hao, and B. Zhang, "Simplified prediction model of frequency nadir for power systems penetrated with renewable energy," in *2022 IEEE Power Energy Society General Meeting (PESGM)*, 2022, pp. 1–5. DOI: 10.1109/PESGM48719.2022.9917200.

[21] North American Electric Reliability Corporation (NERC). "Balancing and Frequency Control." Accessed: 2024-05-12. (May 2021), [Online]. Available: https://www.nerc.com/comm/RSTC_Reliability_Guidelines/Reference_Document_NERC_Balancing_and_Frequency_Control.pdf.

[22] ENTSO-E, "Policy 1: Load-Frequency Control and Performance (Appendix)," European Network of Transmission System Operators for Electricity (ENTSO-E), Tech. Rep., version 1.9, 2004, Accessed: 2025-03-21. [Online]. Available: https://eepublicdownloads.entsoe.eu/clean-documents/pre2015/publications/entsoe/Operation_Handbook/Policy_1_Appendix%20_final.pdf.

[23] A. Boričić, J. L. R. Torres, and M. Popov, "System strength: Classification, evaluation methods, and emerging challenges in ibr-dominated grids," in *2022 IEEE PES Innovative Smart Grid Technologies - Asia (ISGT Asia)*, 2022, pp. 185–189. DOI: 10.1109/ISGTAsia54193.2022.10003499.

[24] W. Zhang, M. Li, and H. Chen, "Hierarchical optimization configuration strategy of synchronous condensers for voltage and frequency stability enhancement in wind power systems," *Electronics*, vol. 13, no. 22, p. 4359, 2024. DOI: 10.3390/electronics13224359. [Online]. Available: https://www.mdpi.com/2079-9292/13/22/4359.

[25] B. B. Adetokun, J. O. Ojo, and C. M. Muriithi, "Reactive power-voltage-based voltage instability sensitivity indices for power grid with increasing renewable energy penetration," *IEEE Access*, vol. 8, pp. 85 401–85 410, 2020. DOI: 10.1109/ACCESS.2020.2992194.

[26] ENTSO-E, *Synchronous condensers*, https://www.entsoe.eu/technopedia/techsheets/synchronous-condenser/, Accessed: 2025-05-06, 2025.

[27] G. Maier and S. Kadam, *Design aspects of synchronous condensers*, https://cse.cigre.org/cse-n035/a1-design-aspects-of-synchronous-condensers.html, Accessed: 2025-03-05, 2023.

[28] P. E. Marken, A. C. Depoian, J. Skliutas, and M. Verrier, "Modern synchronous condenser performance considerations," in *2011 IEEE Power and Energy Society General Meeting*, 2011, pp. 1–5. DOI: 10.1109/PES.2011.6039011.

[29] S. Sriganesh, S. Sivakeerthana, J. Venkatachalam, *et al.*, "A critical analysis of flywheel energy storage role in grid stability and frequency regulation," in *2024 10th International Conference on Electrical Energy Systems (ICEES)*, 2024, pp. 1–7. DOI: 10.1109/ICEES61253.2024.10776868.

[30] "IEEE Recommended Practice for Excitation System Models for Power System Stability Studies," *IEEE Std 421.5-2016 (Revision of IEEE Std 421.5-2005)*, pp. 1–207, 2016. DOI: 10.1109/IEEESTD.2016.7553421.

[31] A. Narula, "Grid-forming wind power plants," Available at https://research.chalmers.se/publication/534815/file/534815_Fulltext.pdf, PhD thesis, Chalmers University of Technology, Gothenburg, Sweden, 2023.

[32] National Electricity System Operator (NESO), *Gb 36 bus electricity transmission network model*, Accessed: 2025-03-30, 2013. [Online]. Available: https://www.neso.energy/publications/gb-36-bus-electricity-transmission-network-model.

[33] H. Tróndheim, *Ensuring Supply Reliability and Grid Stability in a 100% Renewable Electricity Sector in the Faroe Islands*. Springer Theses, 2023. DOI: 10.1007/978-3-031-28368-0.

A

Robust Grid Model in PowerFactory

This part of the Appendix presents results from the three-phase short-circuit analysis that was conducted across the robust grid model in PowerFactory as well as load flow values from the simulations. These results can be observed in Table A.1.

Table A.1: Load flow results and SCC values for the base case of the robust grid model

Zone	Nom. Voltage [kV]	SCC [MVA]	Voltage [p.u.]	Angle [deg]
1	400	11061.78	1.005	24.2
2	400	10702.57	1.011	23.5
3	400	12258.21	1.007	30.5
4	400	10534.64	1.017	20.6
5	400	14917.58	1.005	19.0
6	400	19635.94	1.021	20.8
7	400	19393.99	1.022	21.7
8	400	21387.74	1.023	20.4
9	400	22127.40	1.016	21.0
10	400	21125.62	1.022	24.8
11	400	17899.02	1.009	24.5
12	400	30069.51	1.011	39.5
13	400	27014.31	1.005	23.6
14	400	15101.01	0.998	23.2
14A	400	21842.23	0.999	29.2
15	400	21052.82	0.996	29.7
16	400	30020.82	1.007	36.9
17	400	28660.53	1.004	35.6
18	400	19052.44	1.010	38.6
19	400	23531.13	1.016	49.0
20	400	24943.28	0.999	41.9

Zone	Nom. Voltage [kV]	SCC [MVA]	Voltage [p.u.]	Angle [deg]
21	400	18782.06	1.012	48.5
22	400	21432.79	1.008	49.2
23	400	28988.48	1.003	41.8
24	400	28078.91	1.007	38.4
25	400	18480.23	1.005	54.8
25A	400	19131.28	1.007	49.5
26	400	16397.54	1.004	56.2
27E	400	16641.12	0.998	62.6
27W	400	15521.99	1.000	59.2
28	400	11591.89	0.987	59.5
29	400	14183.38	0.999	62.8
30	400	10355.83	0.993	61.5
31	400	11751.13	1.006	68.0
32	400	9244.73	1.000	78.5
33	400	9251.84	1.000	71.7

B

Islanded Grid Model in PowerFactory

This part of the Appendix summarizes the Islanded Grid model from PowerFactory. Figure B.1 shows the area representation from PowerFactory. Table B.1 displays the total system generation, load and losses. Table B.2 shows the load flow and SCC values from each bus in the system before implementing the SCs. Table B.3 displays the bus type and P_{max} values for all generators. Lastly, Table B.4 shows the active and reactive power demand from all the loads in the model and where they are connected.

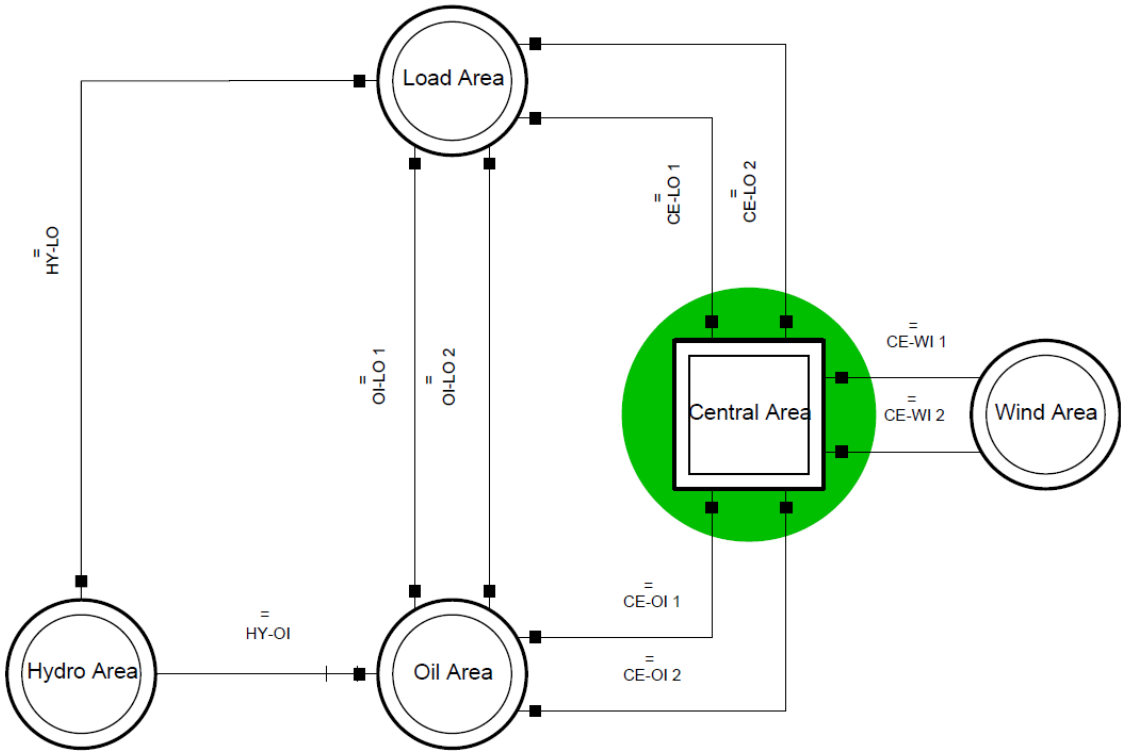

Figure B.1: Islanded grid model from PowerFactory, each area involving the different generators and loads.

Table B.1: Total generation, load and losses in the base case of the islanded grid model

Tot.	P [MW]	Q [MVAr]
Generators	4.0	-0.4
Loads	3.9	1.9
Losses	0.1	-2.2

Table B.2: Load flow results and SCC values for the base case of the islanded grid model.

Area/bus	Nom. Voltage [kV]	SCC [MVA]	Voltage [p.u.]	Angle [deg]
Central area/Bus 1	21	45.01271	0.964	-29.3
Oil area/Bus 2-HV	21	46.61379	0.961	-29.4
Oil area/Bus 2-LV	10.5	43.18296	1.000	0.0
Hydro area/Bus 3	10.5	39.73109	1.013	1.2
Load area/Bus 4-HV	21	44.85185	0.960	-29.4
Load area/Bus 4-LV	10.5	36.10654	1.002	0.1
Wind area/Bus 5.1	21	43.71921	0.965	-29.3
Wind area/Bus 5.2	21	43.83024	0.965	-29.3
Wind area/Bus 5.3	21	43.85494	0.965	-29.3
Wind area/Bus 5.4	21	44.06525	0.965	-29.3
Wind area/Bus 5.5	21	44.08383	0.965	-29.3
Wind area/Bus 5.6	21	44.19546	0.965	-29.3
Wind area/Bus 5.7	21	44.25134	0.965	-29.3

Table B.3: Generation type and rated active power for the respective generators in the base model of the weak grid. Each generator has a power factor of 0.8.

Gen. Names	Bus Type	Gen. Type	P_{max} [MW]
HYDRO G1	PQ	Hydro	1
HYDRO G2	PQ	Hydro	2
OIL G1	Slack	Oil	4.1
WIND T1	PQ	Wind	0.9
WIND T2	PQ	Wind	0.9
WIND T3	PQ	Wind	0.9
WIND T4	PQ	Wind	0.9
WIND T5	PQ	Wind	0.9
WIND T6	PQ	Wind	0.9
WIND T7	PQ	Wind	0.9

Table B.4: Load data and their respective bus connections in the islanded grid model. All loads are modelled as static PQ loads.

Load	**Bus**	P [kW]	Q [kVAr]
L1	2	200	97
L2	2	200	97
L3	2	200	97
L4	2	200	97
L5	2	200	97
L6	2	200	97
L7	2	500	242
L8	3	200	97
L9	4	200	97
L10	4	200	97
L11	4	200	97
L12	4	200	97
L13	4	200	97
L14	4	200	97
L15	4	200	97
L16	4	200	97
L17	4	200	97
L18	4	200	97

DEPARTMENT OF ELECTRICAL ENGINEERING
CHALMERS UNIVERSITY OF TECHNOLOGY
Gothenburg, Sweden
www.chalmers.se

CHALMERS
UNIVERSITY OF TECHNOLOGY